Linking Exponential Components to Kinetic States in Markov Models for Single-Channel Gating

Christopher Shelley and Karl L. Magleby

Department of Physiology and Biophysics and the Neuroscience Program, University of Miami, Miller School of Medicine, Miami, FL 33136

Discrete state Markov models have proven useful for describing the gating of single ion channels. Such models predict that the dwell-time distributions of open and closed interval durations are described by mixtures of exponential components, with the number of exponential components equal to the number of states in the kinetic gating mechanism. Although the exponential components are readily calculated (Colquhoun and Hawkes, 1982, *Phil. Trans. R. Soc. Lond. B.* 300:1–59), there is little practical understanding of the relationship between components and states, as every rate constant in the gating mechanism contributes to each exponential component. We now resolve this problem for simple models. As a tutorial we first illustrate how the dwell-time distribution of all closed intervals arises from the sum of constituent distributions, each arising from a specific gating sequence. The contribution of constituent distributions to the exponential components is then determined, giving the relationship between components and states. Finally, the relationship between components and states is quantified by defining and calculating the linkage of components to states. The relationship between components and states is found to be both intuitive and paradoxical, depending on the ratios of the state lifetimes. Nevertheless, both the intuitive and paradoxical observations can be described within a consistent framework. The approach used here allows the exponential components to be interpreted in terms of underlying states for all possible values of the rate constants, something not previously possible.

The Journal of General Physiology

INTRODUCTION

Ion channels are ubiquitously distributed proteins that control the passive flux of ions through cell membranes by opening and closing (gating) their pores (Hille, 2001). As gatekeepers, ion channels play key roles in many physiological processes, including generation and propagation of action potentials, synaptic transmission, and sensory reception (Hille, 2001). Ion channels gate their pores by passing through a series of conformational states (Jiang et al., 2002; Blunck et al., 2006; Tombola et al., 2006; Purohit et al., 2007). The gating can be described in terms of kinetic reaction schemes that give the number of open and closed states entered during gating, the transition pathways among the states, the rate constants for the transitions, and the voltage and ligand modulation of the rate constants (Colquhoun and Hawkes, 1982, 1995b). Such discrete state Markov models have proven highly useful for describing the underlying gating mechanisms (Horn and Vandenberg, 1984; Zagotta et al., 1994; Cox et al., 1997; Schoppa and Sigworth, 1998; Horrigan et al., 1999; Cox and Aldrich, 2000; Rothberg and Magleby, 1998, 2000; Gil et al., 2001; Zhang et al., 2001; Sigg and Bezanilla, 2003; Chakrapani et al., 2004), and critical tests of single-channel gating for BK channels (McManus and Magleby, 1989) and NMDA receptors (Gibb and Colquhoun, 1992) are consistent with Markov gating.

Single channel recordings from ion channels indicate transitions between open and closed states by characteristic step changes in the single-channel current level. Ion channels can also make transitions among states with the same conductance, such as transitions among closed states and transitions among open states. Connected states of the same conductance are referred to as compound states, and transitions among compound states are hidden because the current level does not change. Nevertheless, information about these hidden transitions is contained in the interval durations, which are lengthened by such transitions.

A standard method used to display data recorded from single channels is to plot the number of observed intervals against their durations, giving open and closed dwell-time histograms, also referred to as dwell-time distributions, or open and closed period distributions. Normalizing the area of the distribution to 1.0 by dividing by the number of intervals in the distribution gives a probability density function, where the area under the curve between any two time values gives the probability of observing an interval with a lifetime (dwell time) between those values (Colquhoun and Hawkes, 1994, 1995b).

Correspondence to Karl L. Magleby: kmagleby@med.miami.edu

The Rockefeller University Press $30.00
J. Gen. Physiol. Vol. 132 No. 2 295–312
www.jgp.org/cgi/doi/10.1085/jgp.200810008

Markov models used to describe single channel kinetics predict that the open and closed dwell-time distributions are comprised of the sums of exponential components (more correctly mixtures because the areas sum to 1.0), with the total number of open and closed exponential components equal to the number of open and closed states, respectively (Colquhoun and Hawkes, 1982, 1995b). Consequently, the experimentally observed dwell-time distributions are typically fit with sums of exponential components to describe the data, such that

$$f(t) = w_1 \exp(-t/\tau_1) + w_2 \exp(-t/\tau_2) + w_3 \exp(-t/\tau_3) + ..., \quad (1)$$

where $f(t)$ is the dwell-time distribution, w_i and τ_i are the magnitude and time constant of each exponential component i, respectively, and t is interval duration. The area of each component, a_i, which gives the number of intervals in that component, is given by $a_i = w_i\tau_i$. It is the exponential components that are typically listed in tables and discussed in papers on single channel kinetics, and the exponential components are often the output (solutions) of gating mechanism calculated with analytical or Q matrix methods (Colquhoun and Hawkes, 1981, 1982, 1995a).

In spite of the emphasis on the exponential components and the many hundreds of papers published with plotted dwell-time distributions and tables of exponential components, there is little practical understanding of how the components relate to specific states in kinetic gating mechanisms (Colquhoun and Hawkes, 1994, 1995b). The reason for this is that all of the rate constants that determine the lifetimes of any of the states in a compound state also contribute to each of the exponential components generated by those states (Colquhoun and Hawkes, 1982, 1995b). Consequently, it is well known for gating mechanisms with compound states that the time constants of the exponential components cannot simply be interpreted as the mean lifetimes of certain states and that the areas of the components cannot be interpreted as the numbers of sojourns to those states (Colquhoun and Hawkes, 1994, 1995b). The problem is further compounded because the methods used to calculate the exponential components from gating mechanisms give little practical information about the relationships between specific components and states. For analytic solutions, which can be derived for models with a limited number of states, the relationship between components and states is obscured in the equations, as shown in the Appendix and Covernton et al., (1994) for a three state model, and in Colquhoun and Hawkes (1977, 1981), Magleby and Pallotta (1983), and Jackson (1997) for more complex models. For the numeric methods that can be used to solve any gating mechanism (Colquhoun and Hawkes, 1981, 1982), there is even less practical information about the contributions of specific states to the various exponential components because of the matrix methods used in the calculations (Horn and Lange, 1983; Colquhoun and Hawkes, 1995a; Colquhoun et al., 1996; Qin et al., 1997).

Hence, the standard dogma is that it is not possible to place physical interpretations on the time constants and magnitudes of the exponential components (Colquhoun and Hawkes, 1995b) except in special cases with extreme differences in some of the rate constants (Colquhoun and Hawkes, 1994), although it should be mentioned that some information relating observed exponentials in experimental data to the underlying states can be obtained when the starting state is known, by examining either first latencies to the next opening/shutting interval or the rise times of macroscopic currents following step changes in agonist concentration or voltage (Edmonds and Colquhoun, 1992; Colquhoun et al., 1996; Wyllie et al., 1998; Horrigan and Aldrich, 2002).

We now present an approach to resolve the relationship between components and states for a model with one open and two closed states in series. We examine simulated gating to determine directly the contributions of the various states to the exponential components, and quantify the contributions in terms of linkage. Our systematic analysis reveals both intuitive and highly paradoxical relationships between components and states, depending on the lifetime ratios of the closed states. Nevertheless, both the intuitive and paradoxical results can be described within a consistent framework.

Our observations should facilitate an understanding of single channel data by providing a physical basis for the origins of the exponential components and of the relationship between components and states. Our observations should also provide sufficient insight to prevent incorrect conclusions when interpreting dwell-time distributions in terms of underlying states and transition probabilities.

Commonly used abbreviations are listed in Table I.

MATERIALS AND METHODS

Using Simulation to Determine the Constituent Dwell-Time Distributions Arising from Designated Gating Sequences for a Three State Model

Colquhoun and Hawkes (1982, 1994, 1995b) have presented detailed methods for calculating the exponential components that sum to describe the dwell-time distributions generated by discrete state Markov models (Colquhoun and Hawkes, 1982, 1994, 1995b). We use their Q-matrix methods (Colquhoun and Hawkes, 1995a) and also their analytical approach (equations in the Appendix) to calculate the exponential components for the models examined. The first step we use to examine the relationship between the exponential components and the underlying states is to determine the specific contributions of the individual states and compound states to the distribution of all closed intervals. Whereas such information can be obtained by the Laplace transform, convolution, and Q matrix methods of Colquhoun and Hawkes (1982), we have chosen to obtain this information by simulating the process by which a hypothetical channel gates, as we found this approach more transparent for revealing the underlying physical basis for the various intervals. This section

TABLE I

Commonly Used Abbreviations

O_1	Open state O_1
C_1, C_2	Closed states C_1 and C_2
t_{C1}, t_{C2}	Mean lifetimes of closed states C_1 and C_2
E_1, E_2	Exponential components E_1 and E_2
τ_{E1}, τ_{E2}	Time constants of exponential components E_1 and E_2
a_{E1}, a_{E2}	Areas of exponential components E_1 and E_2
$\{C_1\}$	Distribution of all closed intervals arising from all sojourns to C_1 in the gating sequence: O_1-C_1-O_1 (see Table II, gating sequence 0). This distribution is a single exponential.
$\{C_1C_2\}$	Distribution of all closed intervals arising from all possible sojourns through both C_1 and C_2 in the gating sequences: O_1-C_1-$(C_2$-C_1-$)_n$-O_1, for $n = 1$ to infinity (see Table II and Eq. 6). This distribution is 0 at zero time, rises with an inflection to a peak, and then decays exponentially at longer times.
$\tau_{\{C1\}}$	Time constant of the $\{C_1\}$ distribution, which is given by t_{C1}
$\tau_{\{C1C2\}}$	Time constant of the decaying phase of the $\{C_1C_2\}$ distribution at long times
$a_{\{C1\}}$	Area of $\{C_1\}$
$a_{\{C1C2\}}$	Area of $\{C_1C_2\}$

describes how the constituent dwell-time distributions that sum to form the dwell-time distribution of all intervals were generated.

The probability for a given gating sequence among states in a kinetic scheme is the product of the probabilities for each of the individual gating steps in the sequence. The probability of a transition from state i to state j, P_{ij}, is given by

$$P_{ij} = k_{ij} / \left(\text{sum of all rate constants away from state } i\right), \quad (2)$$

where k_{ij} is the rate constant from state i to state j (Colquhoun and Hawkes, 1995b).

Consider the following gating mechanism

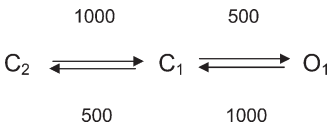

where the rate constants in this scheme (and all following schemes) are in units of per second, and C_2, C_1, and O_1 represent two closed and one open state connected in series, with C_2-C_1 forming a compound state. From this scheme and Eq. 2 the probabilities of various gating transitions and sequences can be calculated. $P_{O1\text{-}C1}$, the probability of the transition from O_1 to C_1 is 1, as there is only one possible route away from O_1, $P_{C1\text{-}O1}$ is 0.5, $P_{C1\text{-}C2}$ is 0.5, and $P_{C2\text{-}C1}$ is 1.0 Thus, the probability of the gating sequence O_1-C_1-O_1 is $1 \times 0.5 = 0.5$. The probability of the gating sequence O_1-C_1-C_2-C_1-O_1 is: $1.0 \times 0.5 \times 1.0 \times 0.5 = 0.25$. Because closed intervals are always initiated by transitions from O_1 to C_1 and always terminate by transitions from C_1 back to O_1, the general case for any gating sequence in the closed states can be abbreviated as C_1-$(C_2$-C_1-$)_n$, where n indicates the number of transitions from C_2 to C_1. The probability of a gating sequence with n transitions from C_2 to C_1, referred to as gating sequence n, is

$$\text{Prob.} \quad \left(C_1\text{-}\left(C_2\text{-}C_1\text{-}\right)_n\right) = \left(P_{C1\text{-}C2}\right)^n \times P_{C1-O1}, \quad (3)$$

where n can have integer values ranging from 0 to infinity. For a sample size of N intervals for all possible gating sequences, each specific constituent distribution $\{C_1\text{-}(C_2\text{-}C_1)_n\}$ for $n = 0$ to effectively infinity (see below) was simulated with $N\times(P_{C1\text{-}C2})^n\times P_{C1\text{-}O1}$ random intervals of duration

$$\sum_{j=1}^{n+1} d_{C1} + \sum_{k=1}^{n} d_{C2},$$

where d_{C1} and d_{C2} are random dwell times described by

$$d_{C1} = -t_{C1} \times \log_e(Rnd) \quad (4)$$

$$d_{C2} = -t_{C2} \times \log_e(Rnd), \quad (5)$$

where t_{C1} and t_{C2} are the mean lifetimes of states C_1 and C_2, and *Rnd* is a random number between 0 and 1. N is typically 10^7 for the simulations.

When $n = 0$, the constituent distribution includes all unitary sojourns to C_1 and is designated $\{C_1\}$; there are no transitions to C_2. In contrast, for values of n between 1 and infinity, each interval results from the sum of 2n+1 exponentially distributed dwell times. Consequently, the constituent distribution $\{C_1\text{-}(C_2\text{-}C_1\text{-})_n\}$ for each value of n is described by the convolution of 2n+1 exponential distributions. (Convolutions are discussed in Colquhoun and Hawkes (1995b).) Unlike exponentials, which have a maximum amplitude at zero time, convolutions have a zero magnitude at zero time, increase to a maximum, and then decay (Colquhoun and Hawkes, 1995b).

The sum of all the constituent distributions for values of n from 1 to infinity will be designated as $\{C_1C_2\}$, as all intervals in this distribution arise from one or more sojourns to both C_1 and C_2. $\{C_1C_2\}$ is calculated with an algorithm that sums all of the constituent distributions.

$$\left\{C_1C_2\right\} = \sum_{n=1}^{\infty} \left\{C_1\text{-}\left(C_2\text{-}C_1\text{-}\right)_n\right\} \quad (6)$$

Because the $\{C_1\}$ and $\{C_1C_2\}$ constituent distributions include the closed intervals from all possible gating sequences, the sum of $\{C_1\}$ and $\{C_1C_2\}$ will give the dwell-time distribution for all observed closed intervals. This is the frequency histogram that would be observed experimentally, assuming that all closings are detected. Dividing the number of intervals in each constituent distribution by N, the total number of closed intervals in all constituent distributions, gives the fraction of all intervals in each constituent distribution. Dividing the number of intervals in each bin of the distribution of all closed intervals by N converts the distribution to a probability density function with an area of 1.

In theory, n should go to infinity in Eq. 6, but in practice, to include all gating sequences with a probability of occurrence of $>10^{-9}$, the maximum needed value of n is given by: $-9/(\log 10(P_{C1\text{-}C2}))$. When $P_{C1\text{-}C2} = 0.5$, $n_{max} \sim 30$. Note the parallel between the analytical Eqs. 149 and 150 of Colquhoun and Hawkes (Colquhoun and Hawkes, 1995b) and the approach described above to generate the various distributions by simulation. The above example of simulating the dwell-time distributions of intervals for each specific gating sequence for a three-state model is also extended to a four state model and could be extended to any gating sequence. The methods used to simulate the single channel current records have been described previously (Blatz and Magleby, 1986).

RESULTS

For a Two-State Model there Is Exact Linkage between Exponential Components and Kinetic States

To approach the question of the relationship between components and states, we start with the simplest possible

model for a channel that can gate its pore, having one open and one closed state (Scheme 1). Infinite frequency response is assumed so that all intervals are detected.

$$C_1 \underset{1000}{\overset{1000}{\rightleftharpoons}} O_1 \qquad \text{(SCHEME 1)}$$

In this example, both the opening and closing rate constants are 1,000/s, giving mean lifetimes (dwell times) of 1 ms for both the open and closed states.

Fig. 1 A presents an example of simulated single-channel data for the gating mechanism described by Scheme 1. The wide range of durations of the open and closed intervals reflect natural stochastic variation arising from the exponentially distributed dwell times in states of Markov models (Colquhoun and Hawkes, 1995b). As a typical first step in analysis, single-channel current records like that in Fig. 1 A, but of much longer duration, are sampled to determine the durations of the open and closed intervals. These durations are then binned into frequency histograms (dwell-time distributions) and fitted with sums of exponential components to quantify the description of the data. For Scheme 1, the open and closed dwell-time distributions are the same because of identical closing and opening rates, so only the closed distribution will be shown. Fig. 1 (B and C) plots the closed dwell-time distribution in two different ways often used in single-channel analysis. Both distributions use log binning so that bin width increases geometrically with time. Log binning gives the ability to quantify interval durations ranging from picoseconds to the age of the universe with constant minimal error in just a few hundred bins (McManus et al., 1987). Fig. 1 B presents the data plotted with the Sigworth and Sine (1987) transform, in which the square root of the number of intervals per bin is plotted against mean bin time on a log scale. The log binning gives a constant apparent bin width on the logarithmic abscissa. Fig. 1 C presents the data displayed on linear coordinates, where the abscissa indicates the mid time of each bin and the ordinate indicates the numbers of intervals per microsecond of bin width, rather than intervals per bin, to transform the log-binned data to the appearance it would have on linear coordinates with constant bin width.

The distributions using either the linear or the Sigworth and Sine transforms are described by a single exponential (continuous lines) with a time constant of 1 ms (arrows). Whereas the Sigworth and Sine plots are highly useful in indicating the time constant of the distribution of intervals by the time at the peak of the distribution, it needs to be remembered in the interpretation of single-channel data that such plots are transforms. The actual distribution of dwell times from a discrete state are like that in Fig. 1 C; the shorter the duration of the interval the greater the frequency of occurrence. It is the exponentially distributed dwell times shown in Fig. 1 (B and C) that give rise to the wide variation in interval durations in Fig. 1 A.

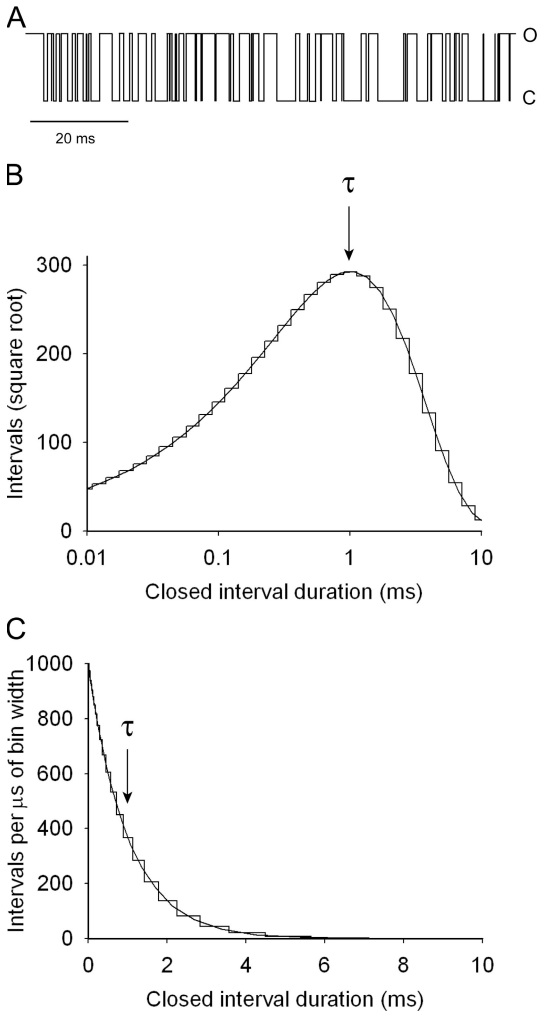

Figure 1. Simulated single-channel data and closed dwell-time distributions for the two state model described by Scheme 1. (A) Simulated single-channel current record with both opening and closing rates constants set to 1,000/s. Channel openings are shown as upward steps. (B) Sigworth and Sine (1987) plot of the closed dwell-time distribution for 10^6 simulated intervals. The distribution is described by a single exponential (continuous black line). The time constant (arrow at 1 ms) falls at the peak of the distribution due to the transform of the data. (C) Same data as in B on linear coordinates. The linear plot reveals the exponential nature of the data: the briefer the interval duration, the greater the number of observed intervals. The arrow indicates the time constant of 1 ms, which indicates the mean duration of the intervals in the distribution, given by the time at which the initial magnitude of the distribution decays to 1/e.

For Scheme 1 with one open and one closed state and perfect time resolution, the closed exponential component would arise entirely from and include all sojourns to C_1, and the open exponential component would arise entirely from and include all sojourns to O_1. Hence,

there is perfect linkage between the exponential components and states.

For Kinetic Schemes with a Compound State, Exponential Components Are Not Directly Linked to Kinetic States

To determine the effect of a compound state on the relationship between components and states, we examined a linear gating mechanism with two closed states in series, as described by Scheme 2.

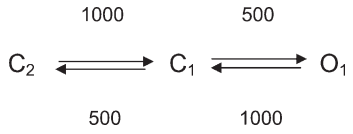

(SCHEME 2)

As with Scheme 1, each state has a mean lifetime of 1 ms. The two connected closed states C_1 and C_2 in Scheme 2 form a compound closed state. Compound states arise when transitions can occur directly between two or more states of indistinguishable conductance. Simulated single channel records from Scheme 2 are shown in Fig. 2 A, where there are brief duration closed intervals, as in Fig. 1 A, and also longer duration closed intervals. As was the case for Scheme 1, which also had one open state, the open dwell-time distribution would be described by a single exponential component with a time constant identical to the mean lifetime of the open state and would be identical to the distributions in Fig. 1 (B and C). The closed dwell-time distribution from Scheme 2 is shown in Fig. 2 B for the Sigworth and Sine transform and in Fig. 2 C for linear coordinates. In contrast to the single exponential for Scheme 1, the closed dwell-time distribution for Scheme 2 (continuous line) is now described by the sum of two exponential components, E_1 and E_2 (dashed lines), with time constants of 0.586 ms and 3.41 ms (arrows) and areas of 0.146 and 0.854, respectively. Neither of these time constants match the 1-ms mean lifetime of either closed state. Hence, when a kinetic scheme contains a compound state, exponential components are not necessarily directly linked to states, as previously noted (Colquhoun and Hawkes, 1994, 1995b).

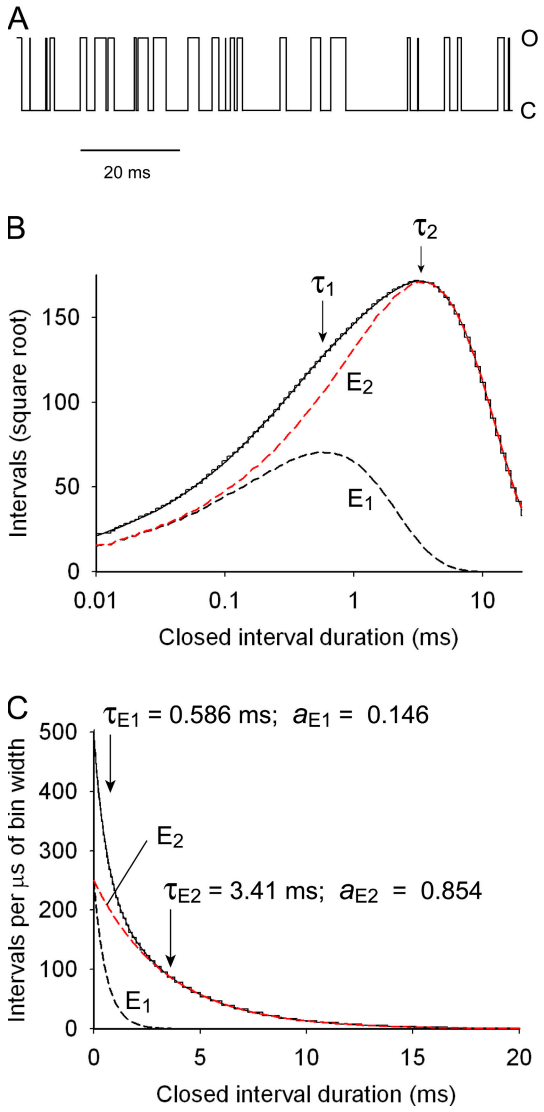

Figure 2. Simulated single-channel data and closed dwell-time distributions for the three-state model described by Scheme 2. (A) Simulated single-channel current record. Channel openings are shown as upward steps. (B) Sigworth and Sine plot of the closed-dwell time distribution for 10^6 simulated intervals. (C) Same data as in B on linear coordinates. The dashed lines in both plots indicate the fast E_1 and slow E_2 exponential components. The time constants (arrows) and areas, which are identical in both B and C, are listed.

The Contribution of Specific Gating Sequences to the Dwell-Time Distribution of All Closed Intervals

To explore the relationship between exponential components and states, the origin of the intervals in the closed dwell-time distribution generated by Scheme 2 was examined. Each closed interval arises from either a unitary sojourn to C_1 or a compound sojourn that includes both C_1 and C_2. In a unitary sojourn, the closed interval is initiated by entry from O_1 into C_1 and is then terminated by a transition from C_1 to O_1 without ever transitioning to C_2, as indicated by gating sequence 0 in Table II. The constituent dwell-time distribution of all such unitary sojourns when $n = 0$ is designated $\{C_1\}$ and can be calculated as described in the Materials and methods. For Scheme 2 the probability of a unitary sojourn is 0.5 (Table II), indicating that half of all closed intervals are in $\{C_1\}$.

For a compound sojourn, the initiation of the closed interval starts the same as for a unitary sojourn, by a transition from O_1 to C_1. Each closed interval is then extended by one or more repeated transitions from C_1 to C_2 and back to C_1 before termination by a transition to O_1. The gating sequences and also the probabilities of

TABLE II

Gating Sequences for Scheme 2, their Probabilities, and State Composition

n	Gating sequence	P	No. of C_1	No. of C_2
0	O_1-C_1-O_1	0.5	1	0
1	O_1-C_1-(C_2-C_1-)$_1$-O_1	0.25	2	1
2	O_1-C_1-(C_2-C_1-)$_2$-O_1	0.125	3	2
3	O_1-C_1-(C_2-C_1-)$_3$-O_1	0.0625	4	3
n	O_1-C_1-(C_2-C_1-)$_n$-O_1	0.5^{n+1}	n+1	n

P is the probability of the indicated gating sequences out of all possible gating sequences for $n = 0$ to infinity. The $\{C_1\}$ distribution is comprised of all closed intervals arising from gating sequence $n = 0$, and the $\{C_1C_2\}$ distribution is comprised of all closed intervals for gating sequences for integer values of $n =$ 1 to infinity (Eq. 6). The sum of the probabilities for gating sequences 1 through infinity is 0.5. Thus, half of all closed intervals are to $\{C_1\}$ with the other half to $\{C_1C_2\}$. No. of C_1 and No. of C_2 indicate the number of sojourns through C_1 and C_2, respectively, that contribute to each interval generated by the specific gating sequence.

compound sojourns arising from 1, 2, or 3 repeated sojourns to C_2, together with the general case gating sequence for n repeated sojourns, are listed in Table II. The constituent dwell-time distribution for each specific gating sequence can be calculated as described in the Materials and methods. The sum of all the constituent dwell-time distributions from all gating sequences for $n = 1$ to infinity in Table II is designated $\{C_1C_2\}$ and can be calculated using Eq. 6 in the Materials and methods. For Scheme 2 the probabilities of the compound gating sequences for $n = 1$ to infinity sum to 0.5, indicating that half of all the closed intervals are in $\{C_1C_2\}$ (Table II).

The $\{C_1\}$ and $\{C_1C_2\}$ distributions are plotted in Fig. 3 (A and B) on linear and semilogarithmic coordinates, respectively, together with the E_1 and E_2 exponential components from Fig. 2. (Recall that an exponential on a plot with a logarithmic ordinate and linear abscissa gives a straight line.) E_1 together with $\{C_1\}$ and E_2 together with $\{C_1C_2\}$ are also plotted in Fig. 3 (C and D), respectively, for ease of comparison. $\{C_1\}$ is a single exponential (green lines) with maximum amplitude at zero time and a time constant of decay of 1 ms, equal to t_{C1}, the mean lifetime of state C_1. In contrast, $\{C_1C_2\}$ has a zero magnitude at zero time, rises with a slight inflection to reach a peak at ~2.5 ms, and then decays, with the decay becoming exponential for durations longer than ~6 ms (blue lines). The $\{C_1C_2\}$ distribution has some characteristics in common with distributions arising from convolutions of exponential functions, because it is comprised of the sum of an infinite number of constituent distributions, each arising from convolutions of exponentially distributed dwell times. Each gating sequence in Table II, as n goes from 1 to infinity, contributes a constituent distribution.

The various constituent distributions for $n = 1$ to 6 in Table II are plotted as numbered purple lines in Fig. 3 B. As n increases, the time to the peak increases, the amplitude of the peak decreases, and the decay after the peak is slower. The increased time to peak and slower decay reflects the increased numbers of sojourns through C_2-C_1 contributing to each closed interval. The decreased amplitudes as n increases reflect that each successive distribution has 50% fewer intervals than the previous one (Table II) and that the interval durations are spread over a greater range (more dwell times contribute to each interval) so that there are fewer intervals of any specific duration. Interestingly, none of the constituent distributions for the individual gating sequences for $n = 1$ to infinity decay exponentially after reaching their peaks, as indicated by the curved decays of the purple lines in Fig. 3 B. However, the sum of all the constituent distributions for the individual gating sequences for $n = 1$ to infinity does decay exponentially, as indicated by the straight line decay of $\{C_1C_2\}$ in Fig. 3 B (blue line) after ~6 ms.

The $\{C_1\}$ and $\{C_1C_2\}$ dwell-time distributions shown in Fig. 3 (A–D) would not be apparent as individual distributions in the experimental data. Rather, $\{C_1\}$ and $\{C_1C_2\}$ sum to form the distribution of all experimentally observed intervals, referred to as the closed dwell-time distribution (continuous black lines in Fig. 3, A and B).

Comparing Exponential Components to States for Scheme 2

To describe the data, the experimentally observed dwell-time distribution would be fitted with the sum of fast and slow exponential components (as in Fig. 2) indicated as E_1 (black dashed lines) and E_2 (red dashed lines) in Fig. 3 (A–D). The predicted dwell-time distribution that would be calculated for Scheme 2 using either Q-matrix or analytical methods would also be given as the sum of the exponential components E_1 and E_2. Hence, both the description of the data and the predicted gating of Scheme 2 would be expressed in terms of the exponential components E_1 and E_2 rather than in terms of the distributions $\{C_1\}$ and $\{C_1C_2\}$ that reflect the actual underlying gating of the channel.

In the interpretation of single-channel data it is sometimes inferred that the $\{C_1\}$ sojourns generate the fast exponential component. A comparison of the $\{C_1\}$ and E_1 distributions in Fig. 3 (A–C), shows that this is not the case for Scheme 2. The area of E_1 is 0.146 and of $\{C_1\}$

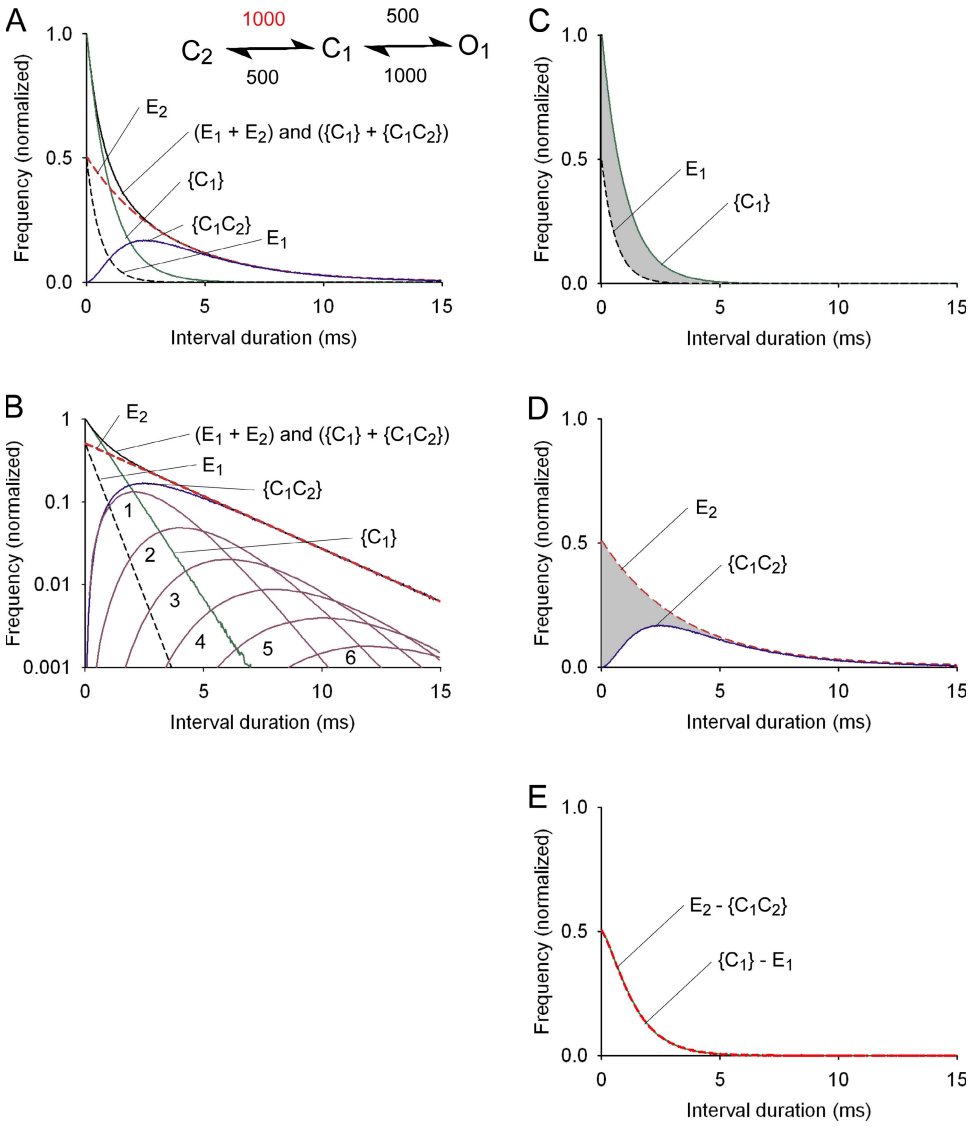

Figure 3. Composition of the dwell-time distribution of all intervals for Scheme 2 in which the t_{C2}/t_{C1} ratio is 1. (A) The observed distribution of all interval durations (black line) is comprised of all $\{C_1\}$ intervals (green line) plus all $\{C_1C_2\}$ intervals (blue line) and is also described by the sum of the exponential components E_1 (black dashed line) plus E_2 (red dashed line). (B) Semilogarithmic plots of the distributions shown in A plus the constituent distributions (purple lines) for specific gating sequences n = 1–6 in Table II, where n indicates the number of C_1 to C_2 transitions for each interval in that distribution. The constituent distributions for n = 1 to infinity sum to generate $\{C_1C_2\}$. (C) The difference between $\{C_1\}$ and E_1 (shaded area) indicates the "excess" intervals in $\{C_1\}$ over those required for E_1. (D) The difference between E_2 and $\{C_1C_2\}$ (shaded area) indicates the "missing" intervals needed to fill in the gap between $\{C_1C_2\}$ and E_2 to complete E_2. (E) A plot of the "missing" intervals, E_2-$\{C_1C_2\}$, exactly superimposes a plot of the "excess" intervals, $\{C_1\}$-E_1, for all interval durations, indicating that the excess intervals are exactly sufficient to fill in the missing intervals at each point in time. Clearly, E_1 is not equal to $\{C_1\}$ and E_2 is not equal to $\{C_1C_2\}$ when the ratio of t_{C2}/t_{C1} is 1. Figs. 3–5 and 8 can be converted into probability density functions by dividing the values on the ordinate by 2.

is 0.5. Thus, no more than 29.2% of the $\{C_1\}$ sojourns could contribute to the E_1 component. In addition, the E_1 intervals have a mean duration of 0.586 ms compared with a mean duration of 1 ms for $\{C_1\}$ sojourns. Hence, E_1 intervals from $\{C_1\}$ would have to be selectively drawn from the briefer intervals in $\{C_1\}$.

In the interpretation of single-channel data it is also sometimes inferred that $\{C_1C_2\}$ sojourns (those sojourns to the compound state C_1C_2) generate the slow exponential component. A comparison of the $\{C_1C_2\}$ and E_2 distributions in Fig. 3 (A, B, and D) indicates that this is also not the case for Scheme 2. Intervals from $\{C_1C_2\}$ do not generate an exponential, but a distribution with zero amplitude at zero time compared with maximum amplitude at 0 time for the E_2 exponential. Consequently, there is a severe deficit of intervals in $\{C_1C_2\}$ at short times compared with E_2 (Fig. 3 D, gray area). For durations >6 ms, however, intervals in $\{C_1C_2\}$ are sufficient to account for the tail of the slow exponential component, as indicated by the superposition of the decay of $\{C_1C_2\}$ and E_2 at longer times (Fig. 3, A, B, and D). Hence, the relationship between components and states changes with the duration of the intervals. At very short times, E_2 arises almost exclusively from $\{C_1\}$, whereas at very long times, E_2 arises almost exclusively from $\{C_1C_2\}$. The lack of direct correspondence between $\{C_1\}$ and E_1 and also between $\{C_1C_2\}$ and E_2 clearly shows that exponential components and kinetic states are not directly linked for Scheme 2.

The Composition of E_1 and E_2 for Scheme 2

Although components and states are not directly linked for Scheme 2, they can be related to each other through the experimentally observed dwell-time distribution of all closed intervals (continuous black lines in Fig. 3, A and B). This distribution can be described in two different

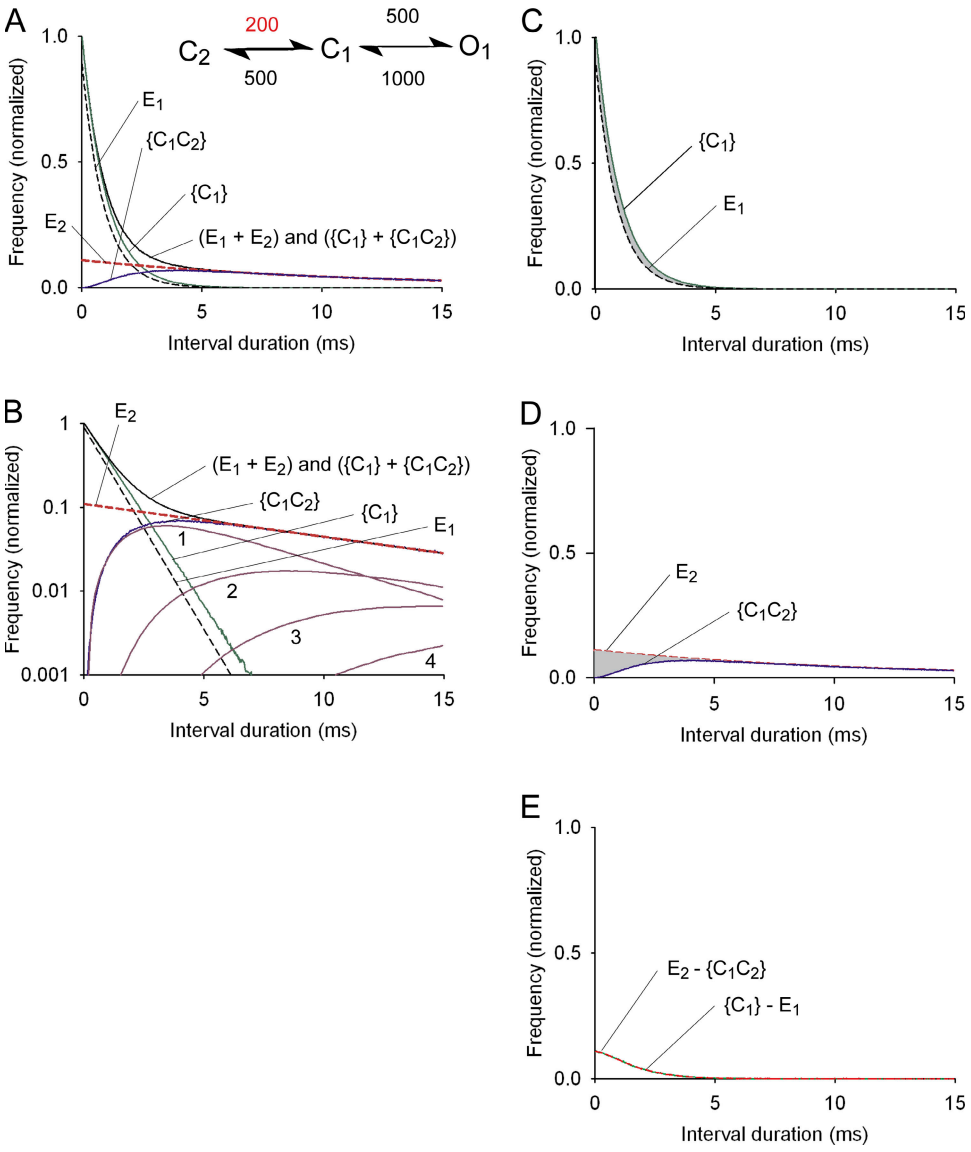

Figure 4. Composition of the dwell-time distribution of all intervals for Scheme 2 in which $k_{C2\text{-}C1}$ is set to 200/s, giving a t_{C2}/t_{C1} ratio of 5. See legend of Fig. 3 for plot details. Compared with Fig. 3 where the t_{C2}/t_{C1} ratio is 1, increasing t_{C2}/t_{C1} fivefold greatly decreases the number of $\{C_1\}$ intervals used to fill in the gap between $\{C_1C_2\}$ and E_2 to complete E_2 at shorter times (gray areas in C and D and plot in E). Consequently, most of the $\{C_1\}$ intervals go to generate E_1 so that E_1 approaches $\{C_1\}$ (compare black dashed and green lines in A–C). Because so few $\{C_1\}$ intervals go to E_2, E_2 is now described by $\{C_1C_2\}$ for all but the shorter duration intervals (compare red dashed line to blue line in A, B, and D).

ways: by the sum of the two exponential components E_1 and E_2, and also by the sum of $\{C_1\}$ and $\{C_1C_2\}$. Thus, for each interval duration in these distributions

$$E_1 + E_2 = \{C_1\} + \{C_1C_2\} \tag{7}$$

and by rearrangement

$$E_2 - \{C_1C_2\} = \{C_1\} - E_1. \tag{8}$$

Fig. 3 D shows that the $\{C_1C_2\}$ and E_2 distributions are identical at longer interval durations but that $\{C_1C_2\}$ is less than E_2 at shorter interval durations. $E_2 - \{C_1C_2\}$ then gives the number of "missing intervals" (Fig. 3 D, shaded area) that would be required to fill in the gap between $\{C_1C_2\}$ and E_2 to complete the E_2 exponential component. Because all intervals in the exponential components arise from $\{C_1\}$ and $\{C_1C_2\}$, the observation in Fig. 3 D that there are insufficient intervals in $\{C_1C_2\}$ to complete E_2 indicates that the missing intervals come from $\{C_1\}$, as there are no other intervals available.

Fig. 3 C shows that the $\{C_1\}$ distribution is greater than the E_1 distribution for all interval durations. Hence, $\{C_1\} - E_1$ indicates the number of "excess intervals" in $\{C_1\}$ that are not required for E_1 (Fig. 3 C, shaded area). Eq. 8 shows that the missing intervals in Fig. 3 D should exactly equal the excess intervals in Fig. 3 C at every point in time. Fig. 3 E shows that this is the case because the lines plotting the numbers of missing and excess intervals superimpose.

Further rearrangement of Eq. 7 indicates the composition of the exponential components

$$E_2 = \{C_1C_2\} + \{C_1\} - E_1 \tag{9}$$

$$E_1 = \{C_1\} - (E_2 - \{C_1C_2\}). \tag{10}$$

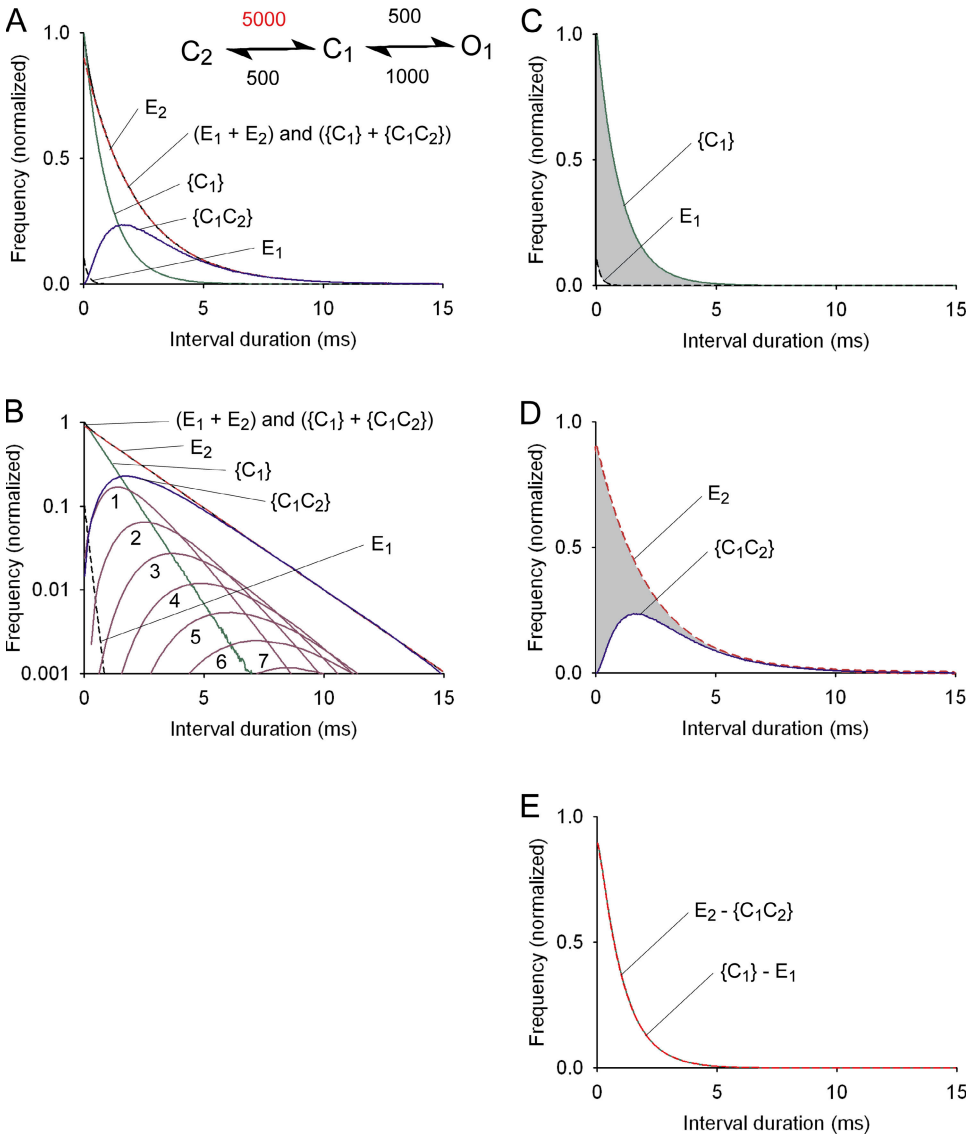

Figure 5. Composition of the dwell-time distribution of all intervals for Scheme 2 in which $k_{C2\text{-}C1}$ is 5,000/s, giving a t_{C2}/t_{C1} ratio of 0.2. See legend of Fig. 3 for plot details. Compared with Fig. 3 where the t_{C2}/t_{C1} ratio 1, decreasing t_{C2}/t_{C1} fivefold greatly increases the number of $\{C_1\}$ intervals needed to fill in the gap between $\{C_1C_2\}$ and E2 to complete E_2 (gray areas in C and D and plot in E). Consequently, most of the $\{C_1\}$ intervals go to E_2, leaving very few $\{C_1\}$ intervals to generate E_1. The net result is that E_1 has a low magnitude and fast time constant (A–C).

Thus, E_2 is comprised of all the $\{C_1C_2\}$ intervals plus those excess intervals in {C1} required to fill in the gap between {C1C2} and E_2 to complete the E_2 exponential, and E_1 is comprised of the leftover intervals in $\{C_1\}$ not used to fill in the E_2 exponential. Because intervals arising from transitions through the compound state C_1C_2 will always form a convolution type of distribution with too few intervals at brief times to complete the E_2 exponential, then some intervals from $\{C_1\}$ will always be required to fill in the E_2 exponential. The fraction of $\{C_1\}$ intervals required to fill in the gap at any point in time depends on interval duration, ranging from 0.5 at zero time to essentially 0 at very long times for Scheme 2 (Fig. 3 D).

Changing the Ratio of the Lifetime of C_2 to C_1 in Scheme 2 while Keeping All Other Aspects of Gating Constant Greatly Alters the Relationship between Components and States

To explore the effect of changing the lifetime of C_2, t_{C2} on the relationship between components and states, t_{C2} in Scheme 2 was altered by changing $k_{C2\text{-}C1}$, the rate constant for the transition from C_2 to C_1. Changing t_{C2} in this manner did not change the lifetime of C_1, t_{C1} (which remained at 1 ms), did not change the probability of entering C_2 from C_1 (which remained at 0.5), did not change the probability of the transition from C_2 to C_1 (which remained at 1), and did not change the relative areas of $\{C_1\}$ and $\{C_1C_2\}$, both of which remained at 0.5. Changing t_{C2} without changing any other aspects of the gating was found to have profound effects on the relationship between components and states.

Results are shown in Fig. 4 for t_{C2} of 5 ms, and in Fig. 5 for t_{C2} of 0.2 ms. These changes in t_{C2} were obtained by changing $k_{C2\text{-}C1}$ in Scheme 2 from 1,000/s to either 200/s or 5,000/s, respectively. The findings in Figs. 4 and 5 should be compared with those in Fig. 3 where t_{C2} was 1 ms. Table III lists the time constants and areas of E_1 and E_2 for these and other values of t_{C2}. Calculations over a wide range of state lifetimes for C_1 and C_2 showed that

TABLE III

Exponential Components and States for Scheme 2 with the Indicated Rate Constants for $k_{C2\text{-}C1}$.

$k_{C2\text{-}C1}$ (s^{-1})	1	10	100	200	1,000	5,000	10,000	100,000
Components and states								
t_{C1} (ms)	1.0	1.0	1.0	1.0	1.0	1.0	1.0	1.0
t_{C2} (ms)	1000	100	10	5	1	0.2	0.1	0.010
τ_{E1} (ms)	0.999	0.995	0.950	0.901	0.586	0.180	0.095	0.010
τ_{E2} (ms)	2001	201.0	21.05	11.10	3.414	2.220	2.105	2.010
a_{E1}	0.499	0.495	0.450	0.402	0.146	0.010	0.0025	0.00003
a_{E2}	0.501	0.505	0.550	0.598	0.854	0.990	0.9975	0.99997
$\tau_{\{C1\}}$ (ms)	1.0	1.0	1.0	1.0	1.0	1.0	1.0	1.0
$\tau_{\{C1C2\}}$ (ms)	The τ of the decay of {C1C2} approaches that of E_2 at longer times							
$a_{\{C1\}}$	0.5	0.5	0.5	0.5	0.5	0.5	0.5	0.5
$a_{\{C1C2\}}$	0.5	0.5	0.5	0.5	0.5	0.5	0.5	0.5

The abbreviations designating the exponential components and states are defined in Table I.

it is the lifetime ratio t_{C2}/t_{C1} rather than the absolute values of the lifetimes that determines the relationship between components and states when the transition probabilities are fixed (not depicted). Consequently, the observations will be discussed in terms of the t_{C2}/t_{C1} ratio in order to make them more general. The t_{C2}/t_{C1} ratios for Figs. 3–5 are 1, 5, and 0.2, respectively.

The key observations to be made from a systematic examination of Figs. 3–5 are as follows.

(a) $\{C_1\}$ (continuous green lines) is identical in each figure (A, B, and C), with a time constant of 1 ms, because changing $k_{C2\text{-}C1}$ has no effect on t_{C1} or on the fraction of intervals in $\{C_1\}$, which remains constant at 0.5.

(b) Increasing t_{C2} fivefold compared with t_{C1} decreases the peak amplitude of $\{C_1C_2\}$ while increasing the time to peak and greatly slowing the decay (compare Fig. 4 to Fig. 3, A, B, and D). These changes in $\{C_1C_2\}$ greatly decrease the deficit of intervals required to fill in the gap between $\{C_1C_2\}$ and E_2 to complete the E_2 exponential at shorter times (compare gray area in Fig. 4 D to Fig. 3 D). Consequently, because fewer $\{C_1\}$ intervals are required to fill in the gap when $t_{C2} >> t_{C1}$, most of the $\{C_1\}$ intervals go to E_1 (compare Fig. 4 C to Fig. 3 C). As a result, the time constant and area of E_1 approach that of $\{C_1\}$ when $t_{C2} >> t_{C1}$ (Fig. 4, A–C; Table III),

(c) In contrast, decreasing t_{C2} fivefold compared with t_{C1} increases the peak amplitude of $\{C_1C_2\}$, while decreasing the time to peak and accelerating the decay (compare Fig. 5 to Fig. 3, A, B, and D). These changes in $\{C_1C_2\}$ greatly increase the number of intervals required to fill in the gap between $\{C_1C_2\}$ and E_2 to complete the E_2 exponential at shorter times (compare gray area in Fig. 5 D to Fig. 3 D). Consequently, because most of the $\{C_1\}$ intervals are required to fill in the missing intervals when $t_{C2} << t_{C1}$, then very few of the $\{C_1\}$ intervals go to E_1 (compare Fig. 5 C to Fig. 3 C). As a result, the time constant and area of E_1 become markedly less than that of $\{C_1\}$ when $t_{C2} << t_{C1}$ (Fig. 5, A–C; Table III), so that E_1 becomes uncoupled from $\{C_1\}$.

(d) That $\{C_1\}$ intervals mainly go to E_1 when $t_{C2} >> t_{C1}$ and to E_2 when $t_{C2} << t_{C1}$ is readily seen by comparing Fig. 4 (C–E) to Fig. 5 (C–E), respectively.

Paradoxical Shifts in the Time Constants and Areas of the Exponential Components as the t_{C2}/t_{C1} Ratio Passes through 1

The observations in Figs. 3–5 and Table III suggest that the relative contribution of the {C1} and $\{C_1C_2\}$ intervals to E_1 and E_2 shifts with the t_{C2}/t_{C1} ratio. To investigate these shifts further, Fig. 6 B plots the time constants of E_1 and E_2, τ_{E1} and τ_{E2}, and the lifetimes of C_1 and C_2, t_{C1} and t_{C2}, and Fig. 6 E plots the areas of E_1, E_2, $\{C_1\}$, and $\{C_1C_2\}$ as $k_{C2\text{-}C1}$ in Scheme 2 is changed over six orders of magnitude to change the t_{C2}/t_{C1} ratio from 10^3 to 10^{-3} (see bottom of Fig. 6). This change in $k_{C2\text{-}C1}$ changes t_{C2} from 1 s to 1 μs (Fig. 6 B, red dashed line) while having no effect on t_{C1}, which remains constant at 1 ms (Fig. 6 B, black continuous line). As t_{C2} decreases, decreasing the t_{C2}/t_{C1} ratio, τ_{E1} first tracks t_{C1} and then switches to track t_{C2} (Fig. 6 B, black dashed line). The switch in tracking occurs as the t_{C2}/t_{C1} ratio passes through 1, with τ_{E1} equal to t_{C1} when $t_{C2} >> t_{C11}$ and then equal to t_{C2} when $t_{C2} << t_{C1}$.

Just as there is a shift in the tracking of τ_{E1} from t_{C1} to t_{C2} as the t_{C2}/t_{C1} ratio passes through 1, there is also a shift in the tracking τ_{E2} from t_{C2} to t_{C1}. τ_{E2} (Fig. 6 B, red continuous line) first tracks t_{C2} when $t_{C2} >> t_{C1}$ and then switches to track t_{C1} when $t_{C2} << t_{C1}$. This tracking occurs with an offset. τ_{E2} is twice t_{C2} when $t_{C2} >> t_{C1}$ and then switches to become twice t_{C1} when $t_{C2} << t_{C1}$.

These paradoxical shifts in the tracking of the time constants are also associated with dramatic shifts in the areas of E_1 and E_2, a_{E1} and a_{E2} (Fig. 6 E). When $t_{C2} >> t_{C1}$, a_{E1} and a_{E2} approach 0.5, essentially the same as the 0.5 areas of $\{C_1\}$ and $\{C_1C_2\}$ (Fig. 6 E, left; Table III). As the t_{C2}/t_{C1} ratio decreases so that $t_{C2} << t_{C1}$, then a_{E1} approaches 0 and a_{E2} approaches 1 (Fig. 6 E, right; Table III). Note that the dramatic shifts in the time constants

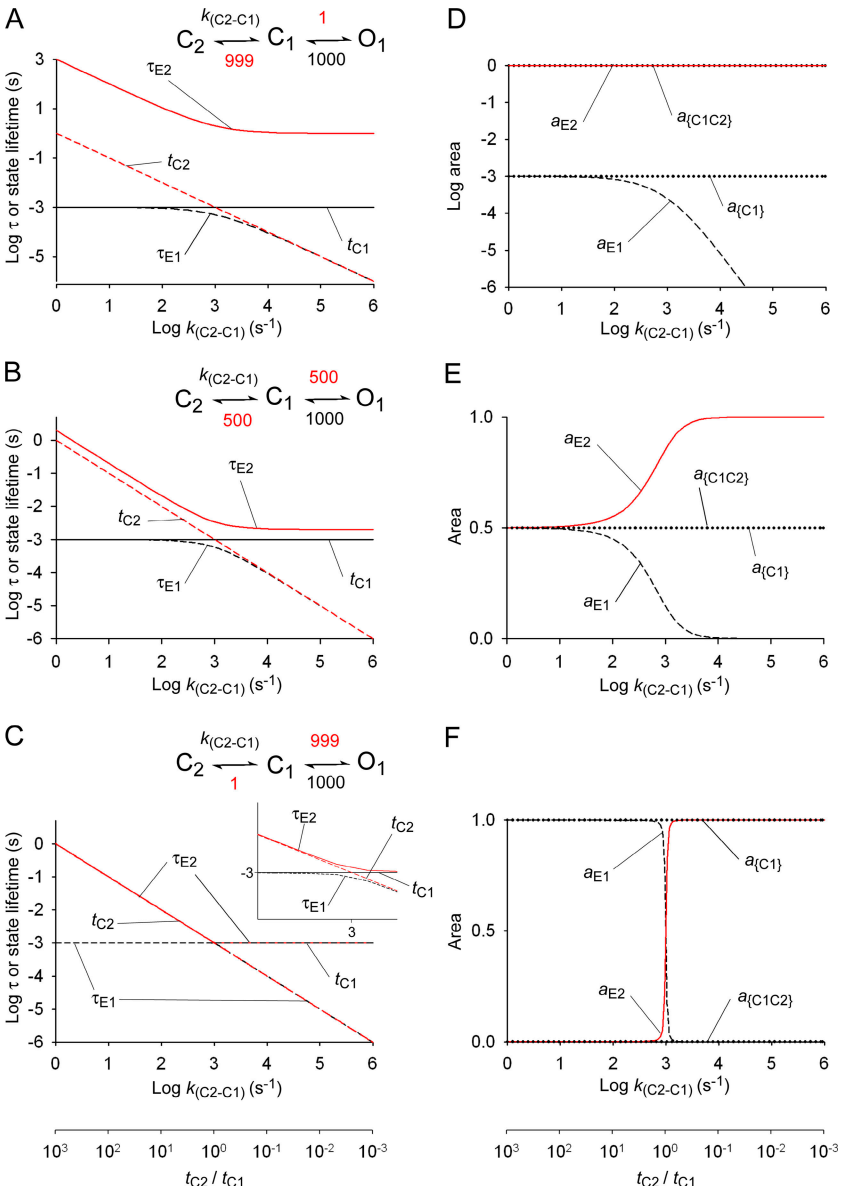

Figure 6. It is the t_{C2}/t_{C1} ratio in Scheme 2 rather than the transition probabilities that determine the paradoxical shifts in the linkage between components and states. (A–C) Plots of τ_{E1} and τ_{E2} against $k_{(C2\text{-}C1)}$ in Scheme 2 as $k_{(C2\text{-}C1)}$ is changed over six orders of magnitude. These changes in $k_{(C2\text{-}C1)}$ change t_{C2} from 1 s to 1 µs as t_{C1} remains constant at 1 ms. The resulting change in the t_{C2}/t_{C1} ratio is plotted at the bottom of the figure. Plots are presented for three different transition probabilities ratios for $P_{C1\text{-}C2}/P_{C1\text{-}O1}$ of 0.999/0.001 (A), 0.5/0.5 (B), and 0.001/0.999 (C). For all three transition probability ratios, τ_{E1} tracks t_{C1} and τ_{E2} tracks t_{C2} (with an offset in A and B) when $t_{C2} >> t_{C1}$ and then τ_{E1} tracks t_{C2} and τ_{E2} tracks t_{C1} (with an offset in A and B) when $t_{C2} << t_{C1}$. The inset in C shows the switch in tracking follows the same pattern as in A and B. (D–F) Areas of E_1, E_2, $\{C_1\}$, and $\{C_1C_2\}$ as a function of $k_{C1\text{-}C2}$ and the resulting t_{C2}/t_{C1} ratio. In D, a log scale is used so that the change in the small area of E_1 can be seen. The corresponding change in the area of E_2 is too small compared with the large area of E_2 to be seen. Note that the paradoxical shifts in time constants and areas of the exponential components as a function of the t_{C2}/t_{C1} ratio are still observed for a 10^6-fold change in transition probabilities.

and areas of E_1 and E_2 occur even though the areas of $\{C_1\}$ and of $\{C_1C_2\}$ remain constant at 0.5 (Fig. 6, B and E; Table III).

The plotted areas in Fig. 6 E quantify the observations shown in Figs. 3–5 (C and D). When $t_{C2} >> t_{C1}$, the areas (and distributions) of E_1 and $\{C_1\}$ are essentially identical and the areas (and distributions) of E_2 and {C1C2} are also essentially identical. When $t_{C2} << t_{C1}$, then the area of E_1 approaches 0 and the area of E_2 approaches the area of $\{C_1\} + \{C_1C_2\}$. Hence, when $t_{C2} >> t_C$ E_1 is comprised of essentially all of the C_1 intervals and E_2 is comprised of essentially all $\{C_1C_2\}$ intervals. The shift in the {C1} intervals from E_1 to E_2 as the lifetime ratio shifts is shown by the decrease in a_{E1} and increase in a_{E2}, such that when $t_{C2} << t_{C1}$ essentially all of the $\{C_1\}$ and $\{C_1C_2\}$ intervals go to E_2.

The paradoxical shifts in the time constants and areas of E_1 and E_2 as the t_{C2}/t_{C1} ratio passes through 1 (Fig. 6, B and E) follow directly from the graphical origins of the exponential components shown in Figs. 3–5 and from the equations in the Appendix. The shifts do not arise from a swapping of the fast and slow exponential components between Eqs. A2 and A3 and Eqs. A4 and A6 in the Appendix, but are self contained in the equation for each component. This is shown graphically in Fig. 6 B, where τ_{E1} is always faster than $\tau_{E2,}$, and in Fig. 6 B by the smooth functions for changes in area. The shifts can be explained visually from the graphical origins of the exponential components detailed in Figs. 3–5. As the t_{C2}/t_{C1} ratio decreases, the shape of $\{C_1C_2\}$ changes so that an increasing number of $\{C_1\}$ intervals are required to fill in the gap between $\{C_1C_2\}$ and E_2 to complete the E_2 exponential, with any leftover $\{C_1\}$ intervals going to generate E_1. It is this shift of $\{C_1\}$ intervals from E_1 to E_2 that shifts the areas and time constants of E_1 and E_2.

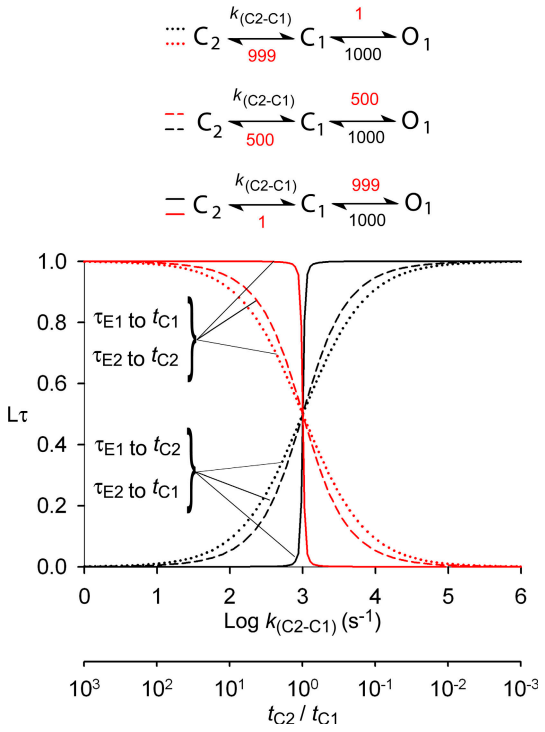

Figure 7. Quantifying the linkage between the time constants of the exponential components and the lifetimes of the states as a function of the t_{C2}/t_{C1} ratio for the three indicated kinetic schemes that encompass a 10^6-fold change in the various transition probabilities away from state C_1. Linkage, Lτ, was calculated with Eq. 11, for the same kinetic schemes as presented in Fig. 6. The paradoxical switch between components and states becomes steeper as the transition probability ratio $P_{C1\text{-}C2}/P_{C1\text{-}O1}$ becomes less, i.e., as the area of $\{C_1C_2\}$ decreases compared with the area of $\{C_1\}$.

Why τ_{E2} Tracks t_{C2} when $t_{C2} >> t_{C1}$ and then Tracks t_{C1} when $t_{C2} << t_{C1}$

The time constant of E_2 tracks t_{C2} (with an offset) when $t_{C2} >> t_{C1}$ (Fig. 6 B) because under these conditions the number of intervals required to fill in the gap between $\{C_1C_2\}$ and E_2 is negligible so that essentially all of the intervals in E_2 arise from $\{C_1C_2\}$ (Fig. 4 and Fig. 6 B), where the duration of C_1 is negligible because $t_{C2} >> t_{C1}$. That the offset for τ_{E2} is twice t_{C2} when $t_{C2} >> t_{C1}$ (Fig. 6 B) is readily calculated from Table II by setting t_{C1} to zero and then calculating the mean closed interval duration (which gives the time constant of E_2) for gating sequences of $n = 1$ to infinity. Note that n starts at 1 because there are essentially no $\{C_1\}$ intervals in E_2 when $t_{C2} >> t_{C1}$. The tracking occurs with an offset equal to twice the duration of t_{C2} because the average number of sojourns through C_2 for intervals generated by gating sequences 1 to infinity is 2.

As t_{C2} becomes less than t_{C1}, τ_{E2} switches over to track t_{C1} (Fig. 6 B). The tracking now occurs with a time constant equal to twice t_{C1} rather than t_{C2}, because when $t_{C2} << t_{C1}$, all of the $\{C_1\}$ and $\{C_1C_2\}$ intervals go to E_2 (Fig. 5 and Fig. 6 E), with the sojourns to C_2 having such brief durations that the dwell time in C_2 does not contribute to interval duration. That τ_{E2} is twice t_{C1} when $t_{C2} << t_{C1}$ (Fig. 6 B) is readily calculated from Table II by setting t_{C2} to zero and calculating the mean closed interval duration for $n = 0$ to infinity, with n starting at 0 because essentially all $\{C_1\}$ and $\{C_1C_2\}$ intervals go to E_2. Thus, the paradoxical shift in the tracking of τ_{E2} from twice t_{C2} when $t_{C2} >> t_{C1}$ to twice t_{C1} when $t_{C2} << t_{C1}$, as determined by the equations in the Appendix, is readily accounted for mechanistically as well as analytically.

Why τ_{E1} Tracks t_{C1} when $t_{C2} >> t_{C1}$ and then Tracks t_{C2} when $t_{C2} << t_{C1}$

The time constant of E_1 directly tracks t_{C1} when $t_{C2} >> t_{C1}$ (Fig. 6 B), because under these conditions an insignificant number of intervals in $\{C_1\}$ are required to fill in the gap between $\{C_1C_2\}$ and E_2, so (essentially) all $\{C_1\}$ intervals go to E_1 (Fig. 4 and Fig. 6 B). Consequently, when $t_{C2} >> t_{C1}$, E_1 and $\{C_1\}$ become synonymous (they contain the same numbers and durations of intervals) so that τ_{E1} directly tracks and is equal to t_{C1}. As t_{C2} becomes less than t_{C1}, τ_{E1} switches over to track t_{C2} (Fig. 6 B) because the majority of the $\{C_1\}$ intervals now go to fill in the gap between $\{C_1C_2\}$ and E_2 to complete the E_2 exponential so that they are no longer available for E1 (Figs. 5 and 6). Interestingly, the few remaining intervals in $\{C_1\}$ left to generate E_1 have a lifetime equal to t_{C2}. It is not readily apparent why this is the case, but it can be shown by numerical substitution into Eq. A2 (Appendix) that when $k_{+1} >> (\beta + k_1)$, i.e., when $t_{C2} << t_{C1}$, then $\tau_{E1} \sim 1/(k_{+1})$, i.e., $\tau_{E1} \sim t_{C2}$.

Generalizing the Observations for All Transition Probabilities

Figs. 3–5 and Fig. 6 (B and E) examined the relationship between components and states as a function of the t_{C2}/t_{C1} ratio for the specific case of equal transition probabilities away from state C_1 in Scheme 2 where $P_{C1\text{-}C2}$ is equal to $P_{C1\text{-}O1}$, with both equal to 0.5. This section examines whether the same general relationship between components and states holds when the ratio of the two transition probabilities away from C_1 is changed over six orders of magnitude. Data are presented for transition probability ratios of $P_{C1\text{-}C2}/P_{C1\text{-}O1}$ of 0.999/0.001 (Fig. 6, A and D) and of 0.001/0.999 (Fig. 6, C and F) for comparison to data for the transition probability ratio of 0.5/0.5 in Fig. 6, B and E).

A comparison of the data for these three markedly different transition probability ratios shows that the paradoxical shifts in the relationship between time constants of exponential components and state lifetimes occurs independently of the transition probability ratio of $P_{C1\text{-}C2}/P_{C1\text{-}O1}$. For the three transition probability ratios considered that span six orders of magnitude

(upper, middle, and lower parts) and for changes in t_{C2}/t_{C1} also over six orders of magnitude (abscissa), τ_{E2} first tracks t_{C2} and then switches to track t_{C1}, whereas τ_{E1} first tracks t_{C1} and then switches to track t_{C2}. The only differences in the plots are that the magnitudes of the offset of τ_{E2}, first from t_{C2} and then from t_{C1}, decreases as the transition probability ratio $P_{C1\text{-}C2}/P_{C1\text{-}O1}$ decreases (see below) and the switch in tracking occurs more rapidly. Thus, the same paradoxical shifts in the tracking of the exponential components to the state lifetimes as the t_{C2}/t_{C1} ratio passes through 1 still occur when the transition probability ratio of $P_{C1\text{-}C2}/P_{C1\text{-}O1}$ is changed a million fold. A decreased offset of τ_{E2} from the state lifetimes would be expected as $P_{C1\text{-}C2}/P_{C1\text{-}O1}$ decreases because the average number of repeated transitions through C_1C_2 contributing to each closed interval would decrease, leading to a decreased time constant of E_2. For example, when $P_{C1\text{-}C2}/P_{C1\text{-}O1}$ is 0.999/0.001 so that 999 out of 1,000 transitions away from C_1 are to C_2, then the time constant of E_2 is ~1,000-fold greater than t_{C2} when $t_{C2} >> t_{C1}$ and ~1,000-fold greater than t_{C1} when $t_{C2} << t_{C1}$ (Fig. 6 A). At the other extreme, when $P_{C1\text{-}C2}/P_{C1\text{-}O1}$ is 0.001/0.999 so that only 1 out of 1,000 transitions away from C_1 go to C_2, then the time constant of E_2 is within 0.1% of t_{C2} when $t_{C2} >> t_{C1}$ and within 0.1% of t_{C1} when $t_{C2} << t_{C1}$ (Fig. 6 C).

As more transitions from C_1 are directed to either C_2 or O_1 due to different $P_{C1\text{-}C2}/P_{C1\text{-}O1}$ ratios, the areas of $\{C_1\}$ and $\{C_1C_2\}$ change, as would be expected. For $P_{C1\text{-}C2}/P_{C1\text{-}O1}$ ratios of 0.999/0.001, 0.5/0.5, and 0.001/0.999, the area of $\{C_1C_2\}$ is 0.999, 0.5, and 0.001, and the area of $\{C_1\}$ is 0.001, 0.5, and 0.999, respectively (Fig. 6, D, E, and F, dotted straight lines). These areas remain constant as $k_{C2\text{-}C1}$ is changed. Just as the paradoxical shifts in time constants occur independently of the $P_{C1\text{-}C2}/P_{C1\text{-}O1}$ ratio as the t_{C2}/t_{C1} ratio passes through 1, the paradoxical shifts a_{E1} and a_{E2} also occur independently of the $P_{C1\text{-}C2}/P_{C1\text{-}O1}$ ratio, that is, independently of whether most of the closed intervals arise from $\{C_1\}$ or $\{C_1C_2\}$. When $P_{C1\text{-}C2}/P_{C1\text{-}O1}$ is 0.999/0.001, a_{E1} is small, containing <0.1% of the intervals when $t_{C2} >> t_{C1}$ (Fig. 6 D, left). Yet, these few intervals in E_1 still shift to E_2 as the t_{C2}/t_{C1} ratio passes through 1, as indicated by the decrease in a_{E1} in Fig. 6 D that is apparent because of the log ordinate. The accompanying increase in a_{E2} is not apparent because the fractional increase is small compared with initial large size of a_{E2}. For the reverse situation in which $P_{C1\text{-}C2}/P_{C1\text{-}O1}$ is 0.001/0.999, a_{E1} contains 99.9% of the area and a_{E1} only 0.001% when $t_{C2} >> t_{C1}$ (Fig. 6 F, left). This distribution of areas then fully reverses as the t_{C2}/t_{C1} ratio passes through 1 (Fig. 6 F, right).

The results in Fig. 6 then show that the paradoxical shifts in the relationship between exponential components and states is determined by the lifetime ratio t_{C2}/t_{C1} rather than by the specific lifetimes of the states or the specific transition probabilities.

Quantifying the Linkage between the Time Constants of Exponential Components and Lifetimes of States

If the duration of intervals in an exponential component is determined mainly by the dwell times arising from sojourns through a particular state, then a fractional change in the lifetime of that state should produce the same fractional change in the time constant of the exponential component. Eq. 11 incorporates this rational to quantify the linkage between components and states, Lτ, such that

$$L\tau = \left[(\tau_{Ei}' - \tau_{Ei})/\tau_{Ei}\right] / \left[(t_{Cj}' - t_{Cj})/t_{Cj}\right], \qquad (11)$$

where τ_{Ei} is the time constant of exponential component i when the mean lifetime of state j is t_{Cj}, and τ_{Ei}' is the time constant of exponential component i after the lifetime of state j is changed a small fractional amount to t_{Cj}'. The lifetime of state j is changed without changing the transition probabilities among any of the states by increasing (or decreasing) all of the rate constants leading away from state j by the same small fractional amount (typically 10^{-5}), with τ_{Ei}' and τ_{Ei} calculated using analytical (Appendix) or Q-matrix methods (Colquhoun and Hawkes, 1995a).

Fig. 7 plots linkage as a function of the t_{C2}/t_{C1} ratio for the same three kinetic schemes that were examined in Fig. 6 encompassing a 10^6-fold change in the transition probabilities away from state C_1. When $t_{C2} >> t_{C1}$, there is near perfect linkage of τ_{E1} to t_{C1}, and of τ_{E2} to $t_{C2,}$ as indicated by values for Lτ approaching 1, and essentially no linkage of τ_{E2} to t_{C1}, and of τ_{E1} to t_{C2}, as indicated by values for Lτ approaching 0. The linkages then reverse when $t_{C2} << t_{C1}$, so there is near perfect linkage of τ_{E2} to t_{C1}, and of τ_{E1} to t_{C2} and no linkage of τ_{E1} to t_{C1}, and of τ_{E2} to $t_{C2.}$ The quantified linkage in Fig. 7 is consistent with the observations and mechanisms discussed in the previous figures.

Knowledge of Paradoxical Shifts Can Prevent Misinterpretation of Experimental Observations

Knowledge of the paradoxical shifts shown in Figs. 6 and 7 and their underlying mechanisms can prevent possible misinterpretation of the origin of the exponential components. For example, solving for the exponential components for Scheme 2 when $k_{C2\text{-}C1} = 10^5$/s gives time constants of 0.01 ms for E_1 and 2.01 ms for E_2 (Fig. 6 B, right side, and Table III, far right column). Since t_{C2} is 0.01 ms, the same as τ_{E1}, it might be tempting to speculate that E_1 arises in some manner from single sojourns to C_2, rather than from leftover $\{C_1\}$ intervals, as shown in Fig. 5. However, this cannot be the case, as every sojourn to C_2 requires two sojourns through the 1 ms lifetime C_1 in this example, yielding the slower $\{C_1C_2\}$ distribution (Fig. 5; Table II). Furthermore, the $\{C_1C_2\}$ distribution has a magnitude of 0 at time 0, whereas the magnitude of E_1 is maximal at time 0 (Figs. 3–5). Consequently,

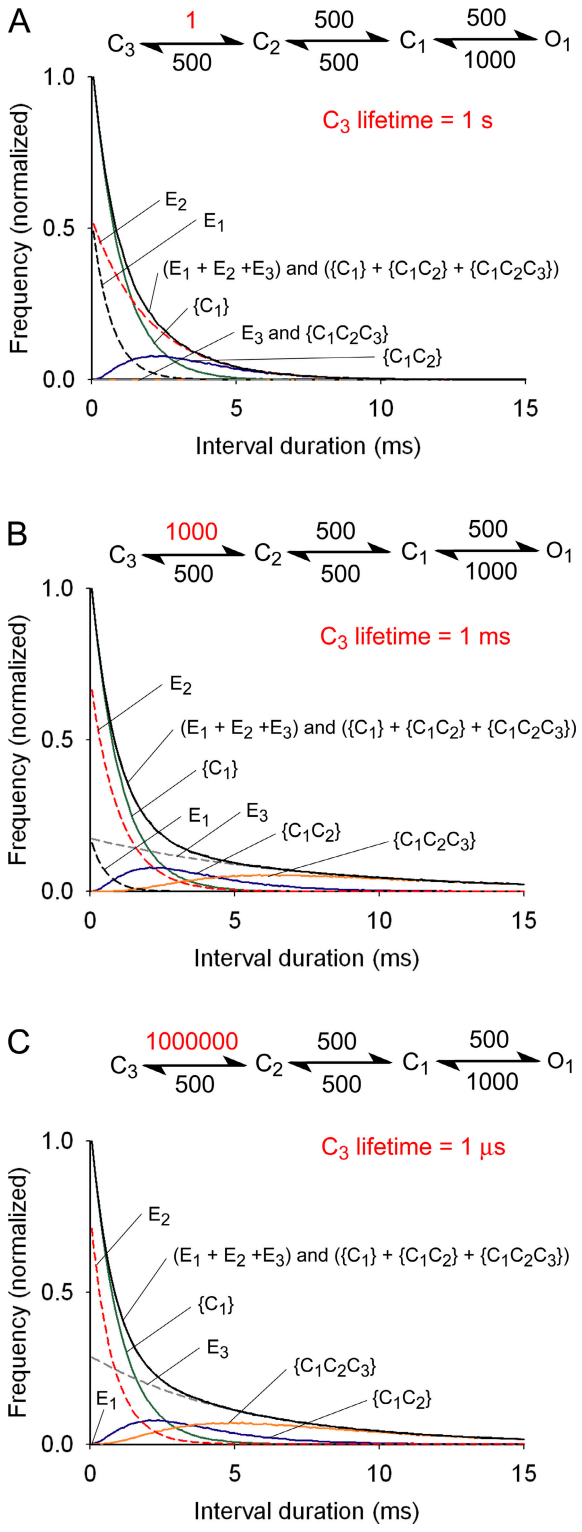

Figure 8. Composition of the dwell-time distribution of all intervals for the indicated four state model when C_3 has a mean lifetime of 1 s (A), 1 ms (B), and 1 µs (C). The time constants (and areas) of the exponential components are (A) E_3: 3003 ms (33.4%); E_2: 2.00 ms (50.0%); E_1: 0.667 ms (16.6%); (B) E_3: 7.46 ms (62.2%); E_2: 1.00 ms (33.3%); E_1: 0.536 ms (4.47%); (C) E_3: 5.24 ms (72.4%); E_2: 0.764 ms (27.6%); E_1: 0.001 ms (~0.00%). The observed distribution of all interval durations (black continuous lines) can be expressed as either the sum of E_1 (black dashed lines), E_2 (red dashed lines), and E3 (gray dashed lines) or as the sum of $\{C_1\}$ (green lines), $\{C_1C_2\}$ (blue lines), and $\{C_1C_2C_3\}$ (orange lines). E_3 is comprised of all intervals from $\{C_1C_2C_3\}$ plus intervals from $\{C_1C_2\}$ and $\{C_1\}$ as needed to complete the E_3 exponential. E_2 is comprised of any leftover intervals from $\{C_1C_2\}$ plus intervals from $\{C_1\}$ as needed to complete the E_2 exponential, and E_1 is comprised of any leftover intervals from $\{C_1\}$.

intervals that include a transition through C_2, i.e., $\{C_1C_2\}$ intervals, cannot be the basis for the very fast E_1 exponential component in this example, no matter how brief the lifetime of C_2. The E_1 component always arises from the same underlying mechanism, no matter what the lifetimes of C_1 and C_2, from the leftover intervals in $\{C_1\}$ not required to fill in the $\{C_1C_2\}$ distribution to complete the E_2 exponential.

Models with Three Closed States in Series

The above sections examined Scheme 2 in which two connected closed states were followed by an open state. We now examine a model with three closed and one open state in series, C_3-C_2-C_1-O_1, which would generate three closed exponential components E_1, E_2, and E_3. Data are presented in Fig. 8 (A–C), where t_{C1} and t_{C2} are both 1 ms for all three schemes, and t_{C3} is 1 s in A, 1 ms in B, and 1 µs in C, changed by altering $k_{C3\text{-}C2}$ as indicated. The transition probabilities $P_{C1\text{-}O1}$, $P_{C1\text{-}C2}$, $P_{C2\text{-}C1}$, and $P_{C2\text{-}C3}$ are the same for the three schemes, with a value of 0.5. For each scheme, intervals from $\{C_1C_2C_3\}$ generate a convolution type distribution analogous to $\{C_1C_2\}$ presented earlier, but with one more closed state contributing to the closed intervals. When t_{C3} is 1 s (A), E_3 and $\{C_1C_2C_3\}$ have long time courses and very low amplitudes so that they run just above the abscissa and are not readily visible. Shortening t_{C3} to 1 ms (B) or 1 µs (C) progressively increases the amplitudes of E_3 and $\{C_1C_2C_3\}$ and speeds their decays. For all three lifetimes of C_3, E_3 superimposes $\{C_1C_2C_3\}$ at longer times, indicating the E_3 arises from $\{C_1C_2C_3\}$ at longer times. Intervals from $\{C_1C_2\}$ and $\{C_1\}$ then fill in the gap between the $\{C_1C_2C_3\}$ distribution and E_3 at shorter times to complete the E_3 exponential. The remaining intervals from $\{C_1C_2\}$ and some of the intervals from $\{C_1\}$ then generate the E_2 exponential, and finally, any remaining intervals in $\{C_1\}$ not used to complete the E_3 and E_2 exponentials generate E_1.

The fraction of intervals in $\{C_1C_2\}$ that go to fill in E_3 and E_2 is highly dependent on the t_{C3}/t_{C2} ratio. When $t_{C3} >> t_{C2}$ (Fig. 8 A), then both E_3 and $\{C_1C_2C_3\}$ are of long duration and very low amplitude so that very few of the $\{C_1C_2\}$ and $\{C_1\}$ intervals are needed to fill in E_3 at shorter times. Consequently, most $\{C_1C_2\}$ intervals go to E_2, with the decay of E_2 superimposing the decay of $\{C_1C_2\}$ at longer times. Intervals from $\{C_1\}$ then fill in the gap between $\{C_1C_2\}$ and E_2 at shorter times to complete E_2, with the leftover intervals from $\{C_1\}$ going to generate

E_1. This distribution of intervals is very similar to Fig. 3 A, except for the addition of the very low amplitude long duration $\{C_1C_2C_3\}$ distribution and E_3 component in Fig. 8 A.

In contrast, when $t_{C3} << t_{C1}$ (Fig. 8 C), then the $\{C_1C_2C_3\}$ distribution has a faster decay and a much higher peak amplitude than in Fig. 8 A, which leads to a major deficit of intervals at shorter times in $\{C_1C_2C_3\}$ compared with E_3. Consequently, large numbers of intervals from $\{C_1C_2\}$ and also from $\{C_1\}$ are required to fill in the gap between $\{C_1C_2C_3\}$ and E_3 at shorter times to complete the E_3 exponential. The consequence of using so many $\{C_1C_2\}$ and also $\{C_1\}$ intervals to complete the E_3 exponential is that there are few leftover $\{C_1C_2\}$ intervals to contribute to E_2. Consequently, E_2 is comprised mainly of the briefer duration $\{C_1\}$ intervals and decays much faster than $\{C_1C_2\}$. Because of the large number of $\{C_1\}$ intervals used for E_3 and E_2 there are essentially no $\{C_1\}$ intervals left to generate E_1, which essentially disappears, having a very fast time constant and essentially no area.

In Fig. 8 B when t_{C3} is 1 ms, intermediate in duration (log scale) between the 1-s lifetime in A and the 1-μs lifetime in part C, then the response is intermediate between those in A and C, with sufficient leftover $\{C_1\}$ intervals to generate a small but detectable E_1. Thus, the same types of paradoxical shifts and underlying mechanisms that generate the exponential components when there are two closed states in series also apply when there are three closed states in series, but with the additional requirement that some of the $\{C_1C_2\}$ and $\{C_1\}$ intervals go to fill in the gap between $\{C_1C_2C_3\}$ and E_3 at shorter times, leaving fewer intervals for E_2 and E_1.

DISCUSSION

Frequency histograms of the number of open and closed intervals vs. their durations are a major means of presenting data recorded from single channels. These dwell-time distributions are typically characterized by fitting with sums of exponential components, as the Markov models used to describe the gating of ion channels predict that such dwell-time distributions would be described by sums of exponential components, with the numbers of components equal to the number of states in the gating mechanism (Colquhoun and Hawkes, 1981, 1982; Magleby and Pallotta, 1983; Colquhoun and Hawkes, 1995a; Jackson, 1997) and Appendix. In spite of the central importance of exponential components to the description of single channel data, little is known about the specific contributions of the various states to each of the exponential components. The question is not whether components can be calculated for a given kinetic scheme, as this is readily accomplished through analytical and Q-matrix methods (Colquhoun and Hawkes, 1982, 1995b), nor is the question the detection of components in histograms, as kinetic mechanisms are typically determined by maximum likelihood fitting of rate constants to data, with the numbers of components implicit in the mechanism being fitted (Horn and Lange, 1983; McManus and Magleby, 1991; Colquhoun et al., 1996). Rather, the question is the physical basis for the exponential components, e.g., what is the state contribution to each component? As long as any discussion of exponential components in terms of underlying gating mechanism is avoided, no specific knowledge is needed. However, in order to relate exponential components to the underlying gating process, it is necessary to understand the relationship between components and states. In this paper we resolve this problem for simple models.

To explore this relationship we examined the simple gating mechanism described by Scheme 2 for two closed and one open state: C_2-C_1-O_1. For this gating mechanism the dwell-time distribution of all closed intervals is described by the sum of fast E_1, and slow E_2 exponential components (Fig. 2). To relate exponential components to underlying states, the closed dwell-time distribution was divided into those intervals arising from single sojourns to C_1 in the gating sequence O_1-C_1-O_1, designated $\{C_1\}$, and into those intervals arising from all sojourns through the compound state C_1-C_2 from the gating sequence O1-C_1-$(C_2$-$C_1)_n$-O1 (where n has integer values from 1 to infinity, Table II), designated $\{C_1C_2\}$.

Graphical Demonstration of the Origin of the Exponential Components from the Underlying States

Our analysis shows that $\{C_1C_2\}$ and E_2 superimpose at longer interval times when the number of {C1} intervals approaches 0 (Figs. 3–5, A–D). This indicates that E_2 at longer times is generated by and includes all intervals from $\{C_1C_2\}$. At shorter interval times, however, there are too few intervals in $\{C_1C_2\}$ to account for E_2 (Figs. 3–5, A, B, and D). To complete E_2 at shorter times, intervals from $\{C_1\}$ fill in the gap between $\{C_1C_2\}$ and E_2, as these are the only other intervals available to do so (Eq. 9, Figs. 3–5, C–E). The leftover intervals in $\{C_1\}$ not used to fill in the gap then generate E_1 (Eq. 10, Figs. 3–5, C–E). This same basic mechanism for the generation of E_1 and E_2 generally applies, independent of the rate constants in Scheme 2 (Figs. 3–5), and allows for a graphical/numerical solution for E_1 and E_2. Although such a procedure would not normally be used, it does illustrate the systematic manner in which the exponential components are generated from the closed states. E_2 is given by the projection of a straight line superimposed at long times on the decay of $\{C_1C_2\}$ plotted on semilogarithmic coordinates (Fig. 3 B, dashed red line superimposed on blue line). $\{C_1C_2\}$ is then subtracted from E_2 to determine the deficit of intervals required to fill in the gap between $\{C_1C_2\}$ and E_2 at shorter times

(Fig. 3 D, gray area). The intervals used to fill the gap, which come from $\{C_1\}$, are then subtracted from $\{C_1\}$ to obtain E_1 (Fig. 3 C). E_1 is then plotted on semilogarithmic coordinates to define its magnitude and time constant (Fig. 3 B, dashed black line). Hence, E_2 arises from all intervals in $\{C_1C_2\}$ plus selected intervals from $\{C_1\}$ as needed to fill the gap, and E_1 arises from the leftover intervals in {C1}.

When Do Exponential Components Equal Kinetic States?

It is sometimes inferred that E_1 is comprised of all of the $\{C_1\}$ intervals and that E_2 is comprised of all the $\{C_1C_2\}$ intervals, so that E_1 is tightly linked to C_1 and E_2 is tightly linked to the compound state C_1C_2. Although the discussion in the previous section indicates that this assumption is not necessarily correct, it would be useful to know under what conditions such an assumption applies. Our analysis shows that there is negligible error associated with this assumption for Scheme 2 when the t_{C2}/t_{C1} ratio is >100 (Figs. 6 and 7; Table III), and that the error remains negligible for 10^6-fold changes in the transition probability ratio of $P_{C1\text{-}O}/P_{C1\text{-}C2}$ (Fig. 6). The errors associated with this assumption become progressively greater as the t_{C2}/t_{C1} ratio decreases. For t_{C2}/t_{C1} and $P_{C1\text{-}O}/P_{C1\text{-}C2}$ ratios of 1, 29% of the $\{C_1\}$ intervals are in E_1 with the rest in E_2 (Table III). As the t_{C2}/t_{C1} ratio becomes <1, the assumption that E_1 is comprised of all the $\{C_1\}$ intervals and that E_2 is comprised of all the $\{C_1C_2\}$ intervals becomes untenable, as the time constant of E_1 switches from tracking t_{C1} to tracking t_{C2}, and the $\{C_1\}$ intervals switch from mainly contributing to E_1 to mainly contributing to E_2 (Figs. 3–7).

This paradoxical switch follows as a simple consequence of the mechanism by which E_1 and E_2 are generated. Because it is the t_{C2}/t_{C1} ratio that determines the magnitude and shape of the $\{C_1C_2\}$ distribution, it is the t_{C2}/t_{C1} ratio that also determines the number of $\{C_1\}$ intervals required to fill in the gap between $\{C_1C_2\}$ and E_2 at shorter times to complete the E_2 exponential (Figs. 3–5, C and D). When $t_{C2} >> t_{C1}$, the relative number of $\{C_1\}$ intervals needed to fill in the gap is insignificant. Consequently, most $\{C_1\}$ intervals go to generate E_1, and E_2 is comprised of mainly $\{C_1C_2\}$ intervals (Figs. 4 and 6). In contrast, when $t_{C2} << t_{C1}$, most of the $\{C_1\}$ intervals are used to fill in the gap between the $\{C_1C_2\}$ distribution and E_2, so there are few intervals available to generate E_1 (Figs. 5 and 6), and this is the case over six orders of magnitude change in the transition probability ratio of $P_{C1\text{-}O}/P_{C1\text{-}C2}$ (Fig. 6, D–F). E_1 has a very small amplitude and very fast time constant when $t_{C2} << t_{C1}$ because essentially all the $\{C_1\}$ intervals go to complete the E_2 exponential at shorter times so that there are few $\{C_1\}$ intervals left to generate E_1 (Fig. 5, C and D; Fig. 6, D–F). Such a change in E_1 can have severe consequences on the interpretation of experimental data, as discussed in the following section.

Difficulty in Detecting Briefer Lifetime Closed States Separated From Open States By Longer Lifetime Closed States

Whereas it is relatively easy to detect slow exponential components of very small areas because of the high likelihood penalties that result if intervals of longer duration are not included in an exponential component (McManus and Magleby, 1988), it is much more difficult to detect fast exponential components of small area superimposed on slower components. For example, when t_{C2} is fivefold less than t_{C1} in Scheme 2, E_1 has a time constant of 0.18 ms and area of 0.01 (Fig. 5, Table III for $k_{C2\text{-}C1}$ of 5,000/s). It is unlikely that such a fast component with only 1% of the area would be detected in experimental data, leading to an incorrect conclusion of a single closed state with a lifetime of 2.22 ms, rather than two closed states with lifetimes of 1 ms (C_1) and 0.2 ms (C_2). It would be even more difficult to detect components arising from briefer duration closed states if there were additional intervening closed states before the open state, as is likely to be the case for data from real channels. Obtaining experimental data over a wide range of conditions that could lead to large changes in state lifetimes, together with simultaneous fitting of the data to gating mechanisms rather than with components could facilitate the detection of states.

Extension to More Complex Gating Mechanisms

The studies in this paper were performed for simple gating mechanisms and for data with perfect time resolution. With limited time resolution, brief duration intervals can go undetected, leading to the formation of compound states that include both open and closed states (Blatz and Magleby, 1986; Hawkes et al., 1992; Colquhoun and Hawkes, 1995b). Such compound states would need to be included when relating exponential components to states. Calculating the fractional change in exponential components for fractional changes in state lifetimes provides a method to examine the linkage between components and states (Eq. 11) for simple as well as highly complex models and also when time resolution is limited.

Understanding the relationship between components and states provides investigators with a physical interpretation for the exponential components in distributions of open and closed dwell times from single channels.

APPENDIX

This section presents the analytical solution for the dwell-time distribution of closed intervals for Scheme 2 following Colquhoun and Hawkes (1981, 1982, 1994). The three rate constants that determine the distribution of closed intervals are designated as:

$$C_2 \underset{k_{-1}}{\overset{k_{+1}}{\rightleftharpoons}} C_1 \overset{\beta}{\rightleftharpoons} O_1$$

The distribution of all closed intervals, $f(t)$, is given by the probability density function described by the sum of two exponential components:

$$f(t) = w_1 \exp(-t/\tau_{E1}) + w_2 \exp(-t/\tau_{E2}), \quad \text{(A1)}$$

where w_1 and w_2 are the magnitudes of the fast E_1 and slow E_2 exponential components, and τ_{E1} and τ_{E2} are the time constants. The time constants, magnitudes, and areas (a) of the exponential components are given by:

$$\tau_{E1} = \frac{2}{\left(k_{+1} + k_{-1} + \beta\right) + \left(\left(k_{+1} + k_{-1} + \beta\right)^2 - 4\beta k_{+1}\right)^{1/2}} \quad \text{(A2)}$$

$$\tau_{E2} = \frac{2}{\left(k_{+1} + k_{-1} + \beta\right) - \left(\left(k_{+1} + k_{-1} + \beta\right)^2 - 4\beta k_{+1}\right)^{1/2}} \quad \text{(A3)}$$

$$w_{E1} = \beta\left(\frac{\left(1/\tau_{E1}\right) - k_{+1}}{\left(1/\tau_{E1}\right) - \left(1/\tau_{E2}\right)}\right); \quad a_{E1} = w_{E1}\tau_{E1}; \quad \text{(A4, A5)}$$

$$w_{E2} = \beta\left(\frac{k_{+1} - \left(1/\tau_{E2}\right)}{\left(1/\tau_{E1}\right) - \left(1/\tau_{E2}\right)}\right); \quad a_{E2} = w_{E2}\tau_{E2}. \quad \text{(A6, A7)}$$

From the analytical solution it can be seen that the time constants, magnitudes, and areas of both E_1 and E_2 are determined by all of the rate constants that affect the lifetimes of both closed states. The relationship between components and states is not readily apparent from these equations, and see also Colquhoun and Hawkes (1981), Magleby and Pallotta (1983), and Jackson (1997) for analytical solutions of more complex gating mechanisms.

It can be shown by numerical substitution into Eq. A2 (or by setting k_{+1} to 0) that when $k_{+1} << (\beta + k_{-1})$, i.e., when $t_{C2} >> t_{C1}$, that

$$\tau_{E1} \sim 1/(\beta + k_{-1}), \quad \text{(A8)}$$

indicating that τ_{E1} approaches t_{C1} when the t_{C2}/t_{C1} ratio is >>1, as shown in the Results, and see Colquhoun and Hawkes (1994) for an alternative means to express limits for τ_{E1}.

It can also be shown by numerical substitution into Eq. A2 (or by setting k_{-1} and β to 0) that when $k_{+1} >> (\beta + k_{-1})$, i.e., when $t_{C2} << t_{C1}$, that

$$\tau_{E1} \sim 1/(k_{+1}), \quad \text{(A9)}$$

indicating that τ_{E1} approaches t_{C2} when the $t_{C2} << t_{C1}$ ratio is <<1, as shown in the Results.

This work was supported in part by Lois Pope LIFE and American Heart Association, Puerto Rico/Florida Affiliate, Postdoctoral Fellowships to C. Shelley, and grants from the National Institutes of Health (AR32805) and the Muscular Dystrophy Associate to K.L. Magleby.

Olaf S. Andersen served as editor.

Submitted: 24 March 2008
Accepted: 20 June 2008

REFERENCES

Blatz, A.L., and K.L. Magleby. 1986. Correcting single channel data for missed events. *Biophys. J.* 49:967–980.

Blunck, R., J.F. Cordero-Morales, L.G. Cuello, E. Perozo, and F. Bezanilla. 2006. Detection of the opening of the bundle crossing in KcsA with fluorescence lifetime spectroscopy reveals the existence of two gates for ion conduction. *J. Gen. Physiol.* 128:569–581.

Chakrapani, S., T.D. Bailey, and A. Auerbach. 2004. Gating dynamics of the acetylcholine receptor extracellular domain. *J. Gen. Physiol.* 123:341–356.

Colquhoun, D., and A.G. Hawkes. 1977. Relaxation and fluctuations of membrane currents that flow through drug-operated channels. *Proc. R. Soc. Lond. B. Biol. Sci.* 199:231–262.

Colquhoun, D., and A.G. Hawkes. 1981. On the stochastic properties of single ion channels. *Proc. R. Soc. Lond. B. Biol. Sci.* 211:205–235.

Colquhoun, D., and A.G. Hawkes. 1982. On the stochastic properties of bursts of single ion channel openings and of clusters of bursts. *Philos. Trans. R. Soc. Lond. B Biol. Sci.* 300:1–59.

Colquhoun, D., and A.G. Hawkes. 1994. The interpretation of single channel recordings. *In* Microelectrode Techniques: The Plymouth Workshop Handbook. 2nd edition. D.C. Ogden, editor. Company of Biologists, Cambridge. 141–188.

Colquhoun, D., and A.G. Hawkes. 1995a. A Q-matrix cookbook. *In* Single-Channel Recording. B. Sakmann and E. Neher, editors. Plenum Press, New York. 589–633.

Colquhoun, D., and A.G. Hawkes. 1995b. The principles of the stochastic interpretation of ion-channel mechanisms. B. Sakmann and E. Neher, editors. Plenum Press, New York. 397–482.

Colquhoun, D., A.G. Hawkes, and K. Srodzinski. 1996. Joint distributions of apparent open and shut times of single-ion channels and maximum likelihood fitting of mechanisms. *Phil. Trans. R. Soc. Lond. A.* 354:2555–2590.

Covernton, P.J., H. Kojima, L.G. Sivilotti, A.J. Gibb, and D. Colquhoun. 1994. Comparison of neuronal nicotinic receptors in rat sympathetic neurones with subunit pairs expressed in *Xenopus* oocytes. *J. Physiol.* 481 (Pt 1):27–34.

Cox, D.H., and R.W. Aldrich. 2000. Role of the β1 subunit in large-conductance Ca^{2+}-activated K^+ channel gating energetics. Mechanisms of enhanced Ca^{2+} sensitivity. *J. Gen. Physiol.* 116:411–432.

Cox, D.H., J. Cui, and R.W. Aldrich. 1997. Allosteric gating of a large conductance Ca-activated K^+ channel. *J. Gen. Physiol.* 110:257–281.

Edmonds, B., and D. Colquhoun. 1992. Rapid decay of averaged single-channel NMDA receptor activations recorded at low agonist concentration. *Proc. Biol. Sci.* 250:279–286.

Gibb, A.J., and D. Colquhoun. 1992. Activation of *N*-methyl-D-aspartate receptors by L-glutamate in cells dissociated from adult rat hippocampus. *J. Physiol.* 456:143–179.

Gil, Z., K.L. Magleby, and S.D. Silberberg. 2001. Two-dimensional kinetic analysis suggests nonsequential gating of mechanosensitive channels in *Xenopus* oocytes. *Biophys. J.* 81:2082–2099.

Hawkes, A.G., A. Jalali, and D. Colquhoun. 1992. Asymptotic distributions of apparent open times and shut times in a single channel record allowing for the omission of brief events. *Philos. Trans. R. Soc. Lond. B Biol. Sci.* 337:383–404.

Hille, B. 2001. Ion Channels of Excitable Membranes. Sinauer Associates, Sunderland, MA. 814 pp.

Horn, R., and K. Lange. 1983. Estimating kinetic constants from single channel data. *Biophys. J.* 43:207–223.

Horn, R., and C.A. Vandenberg. 1984. Statistical properties of single sodium channels. *J. Gen. Physiol.* 84:505–534.

Horrigan, F.T., J. Cui, and R.W. Aldrich. 1999. Allosteric voltage gating of potassium channels I. Mslo ionic currents in the absence of Ca^{2+}. *J. Gen. Physiol.* 114:277–304.

Horrigan, F.T., and R.W. Aldrich. 2002. Coupling between voltage sensor activation, Ca^{2+} binding and channel opening in large conductance (BK) potassium channels. *J. Gen. Physiol.* 120:267–305.

Jackson, M.B. 1997. Inversion of Markov processes to determine rate constants from single-channel data. *Biophys. J.* 73:1382–1394.

Jiang, Y., A. Lee, J. Chen, M. Cadene, B.T. Chait, and R. MacKinnon. 2002. Crystal structure and mechanism of a calcium-gated potassium channel. *Nature.* 417:515–522.

Magleby, K.L., and B.S. Pallotta. 1983. Calcium dependence of open and shut interval distributions from calcium- activated potassium channels in cultured rat muscle. *J. Physiol.* 344:585–604.

McManus, O.B., A.L. Blatz, and K.L. Magleby. 1987. Sampling, log binning, fitting, and plotting durations of open and shut intervals from single channels and the effects of noise. *Pflugers Arch.* 410:530–553.

McManus, O.B., and K.L. Magleby. 1988. Kinetic states and modes of single large-conductance calcium-activated potassium channels in cultured rat skeletal muscle. *J. Physiol.* 402:79–120.

McManus, O.B., and K.L. Magleby. 1989. Kinetic time constants independent of previous single-channel activity suggest Markov gating for a large conductance Ca-activated K channel. *J. Gen. Physiol.* 94:1037–1070.

McManus, O.B., and K.L. Magleby. 1991. Accounting for the Ca^{2+}-dependent kinetics of single large-conductance Ca^{2+} activated K^+ channels in rat skeletal muscle. *J. Physiol.* 443:739–777.

Purohit, P., A. Mitra, and A. Auerbach. 2007. A stepwise mechanism for acetylcholine receptor channel gating. *Nature.* 446:930–933.

Qin, F., A. Auerbach, and F. Sachs. 1997. Hidden markov modeling for single channel kinetics with filtering and correlated noise. *Biophys. J.* 79:1928–1944.

Rothberg, B.S., and K.L. Magleby. 1998. Kinetic structure of large-conductance Ca^{2+}-activated K+ channels suggests that the gating includes transitions through intermediate or secondary states. A mechanism for flickers. *J. Gen. Physiol.* 111:751–780.

Rothberg, B.S., and K.L. Magleby. 2000. Voltage and Ca^{2+} activation of single large-conductance Ca^{2+}-activated K^+ channels described by a two-tiered allosteric gating mechanism. *J. Gen. Physiol.* 116:75–99.

Schoppa, N.E., and F.J. Sigworth. 1998. Activation of Shaker potassium channels. III. An activation gating model for wild-type and V2 mutant channels. *J. Gen. Physiol.* 111:313–342.

Sigg, D., and F. Bezanilla. 2003. A physical model of potassium channel activation: from energy landscape to gating kinetics. *Biophys. J.* 84:3703–3716.

Sigworth, F.J., and S.M. Sine. 1987. Data transformations for improved display and fitting of single-channel dwell time histograms. *Biophys. J.* 52:1047–1054.

Tombola, F., M.M. Pathak, and E.Y. Isacoff. 2006. How does voltage open an ion channel? *Annu. Rev. Cell Dev. Biol.* 22:23–52.

Wyllie, D.J., P. Béhé, and D. Colquhoun. 1998. Single-channel activations and concentration jumps: comparison of recombinant NR1a/NR2A and NR1a?NR2D NMDA receptors. *J. Physiol.* 510:1–18.

Zagotta, W.N., T. Hoshi, and R.W. Aldrich. 1994. Shaker potassium channel gating. III: Evaluation of kinetic models for activation. *J. Gen. Physiol.* 103:321–362.

Zhang, X., C.R. Solaro, and C.J. Lingle. 2001. Allosteric regulation of BK channel gating by Ca^{2+} and Mg^{2+} through a nonselective, low affinity divalent cation site. *J. Gen. Physiol.* 118:607–636.